PULSE HEIGHT "MULTIPLICATION" IN SURFACE BARRIER DETECTORS

H. Breneman

Space Radiation Laboratory
California Institute of Technology
Pasadena, California

SRL Internal Report #87
February 23, 1982

PULSE HEIGHT "MULTIPLICATION" IN SURFACE BARRIER DETECTORS

H. Breneman

Space Radiation Laboratory
California Institute of Technology
Pasadena, California

SRL Internal Report #87
February 23, 1982

I. INTRODUCTION

Silicon solid-state surface-barrier type detectors have been and continue to be used in many SRL cosmic ray detector systems. It has been observed that these detectors sometimes exhibit a pulse-height "multiplication" effect, in which some of the particles yield pulse heights that are anomalously high (by about 10 - 30 %), the effect occurring most frequently among highly ionizing particles. The effect has been seen both in the laboratory and in flight (Fig. 1); examples can be found in flight data from Voyager LET 35-μm detectors (Ref. 1) and in preflight calibration data for ISEE-3 HIST 150-μm detectors (Ref. 2). The purpose of this report is to describe quantitative measurements of the magnitude of this effect and its dependence on energy, charge and bias voltage for a particular set of detectors, with the object of anticipating, and if possible minimizing, the extent of the problem in future detector systems.

II. DATA DESCRIPTION AND EXPERIMENTAL APPROACH

The detectors used in the study were one 500-μm and four 175-μm surface barrier detectors; along with three additional 500-μm units, they were supplied by Ortec to be used as part of the COMPAS cosmic ray experiment package originally intended for flight on the NASA International Solar Polar Mission spacecraft. Several important detector parameters are listed for all eight detectors in Table I. The data analyzed below were obtained during mapping/calibration tests with an ^{40}Ar beam from the Lawrence Berkeley Laboratory Bevalac in April and June of 1981. The April runs (hereafter referred to as "Berkeley I") involved two different detector "stacks", were done at the manufacturer's recommended operating bias voltage for the detectors and have good event statistics; these runs provide good information on the energy-loss dependence of the effect and on the differences between the detectors. The data collected in June ("Berkeley II"), utilizing a single stack, have poorer statistics and worse background effects but include runs at six biases between the recommended operating bias and the depletion voltage, for each detector. The three stacks are depicted schematically in Fig. 2. Note that all of the surface barrier detectors in all of the stacks were oriented with the gold-coated side facing the beam, except for the reversal of detectors 175-1 and 175-4 in Berkeley II. The bias voltages on all of the detectors in each of the ten runs are given in Table II. The PACE data collection system was used in Berkeley I, while the Berkeley II runs used other laboratory electronics, including an eight-channel PHA system built by W. R. Cook with software devised by A. C. Cummings. Multi-wire proportional counters provided position information in Berkeley I, but no position information was available in Berkeley II.

III. DEPENDENCE ON ENERGY LOSS

The Berkeley runs included pulser calibration data for converting detector pulse heights into absolute energies. Computer software, written in C language, was devised for generating cross-plots and histograms of pulse heights or functions of pulse heights, subject to selected coincidence requirements. In studying the multiplication effect in a given detector, the relevant subset of the data consists of those events which pass completely through the detector under study, losing energy ΔE_1, and stop in the next detector where they lose their remaining energy E'. The multiplication effect can be exhibited by plotting ΔE_1 vs. E' for each detector. Such plots are shown in Figs. 3 - 7 for the five detectors tested using all Berkeley I data meeting the above coincidence requirements. Tracks due to ^{40}Ar, as well as lighter elements produced by fragmentation, are seen; the anomalous ^{40}Ar events appear in the region of Z = 20 to 22 and clearly occur more frequently at higher values of ΔE_1. Of course the effect also occurs for the lighter elements, yielding points that plot in the region normally occupied by elements two or three charge units higher. Note the "double-valued" appearance of the multiplication effect in detector 175-4 (Fig. 6). Anomalous events were not seen for particles stopping within the surface barrier detector; that is, when it served as the E'-detector and another type of detector, not showing the effect, served as the ΔE_1-detector. Bad events were sometimes seen in the E'-detector in the "fold-back" part of the element track, but these are events which have actually penetrated the E'-detector and were left with insufficient energy to trigger the next detector in the stack. An example of this situation appears in Fig. 4. The subject of stopping vs. penetrating events will be discussed in more detail in section V.

Clearly a charge Z calculated from ΔE_1 and E' will be incorrect for the anomalous events. On the other hand, if E' is plotted against the energy loss in an earlier detector which does not show the effect (such as the detector preceding the ΔE_1 detector, to be denoted ΔE_2), the "bad" events will not be evident since only the pulse height in the ΔE_1-detector is in error (see Fig. 8, containing the same events as Fig. 3). The value of Z calculated from ΔE_2 and E' will be accurate for both "good" and "bad" events. Therefore a cross-plot of these two determinations of Z will suffice to separate the "good" and "bad" events for all elements that can be resolved.

The charge Z was calculated from ΔE_1 and E' by using a power-law range-energy relation, $R = (kA/Z^2)\,(E/A)^a$ with the approximation A = 2Z, to generate a "first guess" of the function $Z(\Delta E_1,E')$. This first approximation has the form $Z(\Delta E_1,E') = \text{constant} * [(E'+\Delta E_1)^a-(E')^a]^{\frac{1}{a+1}}$. Empirical corrections to this function were applied iteratively until a plot of $Z(\Delta E_1,E')$ vs. E' gave straight lines for all resolved elements. An example of the final result of this process is shown in Fig. 9, which was derived in this way from Fig. 3. The process was repeated using ΔE_2 instead of ΔE_1 to generate $Z(\Delta E_2,E')$ (see Fig. 10, derived from Fig. 8). The resulting cross-plot of these two determinations of Z is shown in Fig. 11; the corresponding figures for the other three 175-μm detectors appear as Figs. 12 - 14. In these plots the "good" and "bad" events are clearly evident; it is possible to count the number of events in each class by imposing selection criteria that draw a "box" around the good or bad events. One can also consider subsets of the data based on energy, by imposing selection requirements on E'. In this way one can determine the fraction of events which have "bad" ΔE_1 as a function of E' (or "normal" ΔE_1). Fig. 15 is a plot of the bad event fraction (bad events divided by total events) as a function of ΔE_1 for detector 175-2. The Berkeley I data for each of several Z values was divided into several E' bins; the "normal" range of ΔE_1 corresponding to each of these E' intervals was determined from a histogram of a scatter-plot such as Fig. 3. Fig. 15 quantifies what is apparent in the figures already presented, that the occurrence of bad events increases sharply with ΔE_1, and also that different elements show the same general pattern.

It is possible that a parameter related to ΔE_1, such as dE/dx at the front or back surface of the detector, would better correlate with bad event fraction. The fact that the effect is not seen in Berkeley I data until the particles have passed completely through the detector (that is, it is seen only when the 175- or 500-μm detector is the ΔE_1-detector, not the E'-detector) suggests that dE/dx at the back (aluminum) surface of the detector is an important parameter. Accordingly, a C program was written to calculate this quantity from E' for any given ΔE_1-E' combination. This involved calculating range-energy tables for the nuclei of interest from the Janni range-energy tables for protons in silicon (Ref. 3) with the Barkas and Berger corrections for heavy nuclei (Ref. 4), and numerically differentiating these tables, taking into account the air gap between the detectors in the stack. When dE/dx is used instead of ΔE_1 in the plot of bad event fraction, the result is Fig. 16, based on the same data as Fig. 15. Since the bad event fraction is always between 0 and 1, probability graph paper is appropriate here; the results from Berkeley I for each of the four 175-μm detectors, including Z = 18 only, appear in Figs. 17 and 18. Corresponding information for the one 500-μm detector studied in Berkeley I appears in Fig. 19. All five detectors are compared in Fig. 20, with the data points replaced by smooth curves. It can be seen that three of the 175-μm detectors are similar, with only small, possibly insignificant differences, while the fourth (which is also the one showing the "double-valued" multiplication effect) is much worse at high dE/dx. The magnitude of the effect in the 500-μm detector is seen to be much reduced compared to that in any of the 175-μm devices. An inspection of these figures, in particular Figs. 15 and 16, also suggests that there is a threshold below which the multiplication effect does not occur, or at least its occurrence is reduced to the level of other sources of background in the data. From Figs. 15 and 16, this threshold appears to be at a ΔE_1 (in a 175-μm detector) of about 160 MeV, corresponding to a dE/dx at the back of the detector of about 4 - 5 GeV/(g/cm^2). The numerical data from which these figures were derived are tabulated for the five detectors in Tables III - VII.

Having established the relation between dE/dx and bad event fraction for the detectors, it is of interest to know what residual range (i.e., depth in the E'-detector) is implied by a given value of dE/dx and bad event fraction for different elements, if these surface barrier detectors were incorporated in a cosmic ray instrument. The computer program referred to above also calculates residual range from E' by interpolating in the range-energy table. Fig. 21

shows residual range as a function of Z for three different values of dE/dx; the corresponding values of bad event fraction were obtained from the Fig. 20 curve for detector 175-2, a typical case. It can be seen that for Fe, for example, events stopping in the first 2 mm of E'-detector will contain at least 2% exhibiting the multiplication effect; in the first 400 μm the fraction is about 30%, and in the first 100 μm the fraction rises to almost 90%. The situation is clearly even worse at higher Z; the 2 mm of residual range that gives 2% bad events at Z = 26 gives 30% at Z = 40. Since 2 mm is approximately the maximum residual range for which the pulse height in this detector would be used, the problem is a serious one and demonstrates the importance of finding out what variables will reduce the incidence of the effect, so as to minimize the problem if possible.

IV. DEPENDENCE ON BIAS VOLTAGE

It had been previously noted that the multiplication effect occurred most often in those SRL surface-barrier detectors with the highest average internal electric field strengths (Fig. 22). This suggested that lowering the detector bias voltage might reduce the incidence of the effect in a given detector. Since the recommended operating voltage is substantially above the depletion voltage for such detectors (see Table I for example), there is a considerable range of possible voltages within which the detector can be successfully operated.

To examine the impact on the multiplication effect of reducing detector bias, it is necessary to make use of the Berkeley II data. Since the event statistics are much poorer here than in Berkeley I, the approach used before, of generating a curve of bad event fraction vs. dE/dx by breaking up each range into subintervals of energy, was not used here. Instead, the curves of bad event fraction obtained from Berkeley I were viewed as defining the *probability* for an event with given dE/dx to be a bad event, for a particular ΔE_1-detector operating at full bias. For all events in Berkeley II having that same ΔE_1-detector, a value of dE/dx could be calculated in the same manner as before, and using the Berkeley I curve (with suitable interpolation) a "probability of being bad" could be assigned to every event, both good and bad. The sum of these probabilities is the "expected number of bad events" for that data set; this can be compared with the actual number of bad events obtained by counting events in a box on a cross-plot of two Z-determinations, as described in Section III. For Berkeley II runs at normal bias, the predicted and observed numbers of bad events should agree to within statistical accuracy. If the predicted and observed values consistently disagree to within statistics for low-bias runs, one can conclude that reducing detector bias has an effect on the occurrence of the bad events. On account of the small magnitude of the multiplication effect in the 500-μm detector and the overall poorer statistics in Berkeley II, these calculations were performed only for data subsets in which the 175-μm detectors were the ΔE_1-detector.

As in Berkeley I, cross-plots of $Z(\Delta E_2,E')$ vs. $Z(\Delta E_1,E')$ were prepared for each case, in the manner described in Section III. These plots, which include data for all six biases, appear as Figs. 23 - 26. The poorer statistics and worse background effects in Berkeley II are apparent (compare with Figs. 11 - 14); in many cases the "bad" events do not stand out in a well-defined cluster as in Berkeley I. Accordingly, the location of the bad-event "box", for defining actual bad events in Berkeley II, was set by reference to the corresponding plot in Berkeley I (Figs. 11 - 14). The worse background in Berkeley II may be related to the higher event rates experienced in these runs, the stack geometry or the data collection system used instead of PACE. For every case except detector 175-2, only Z = 18 events were used in Berkeley II; the data for lower charges were obscured by background effects, primarily edge effects (see for example Fig. 23). For detector 175-2, the data for lower charges were "cleaner" and Z = 14 through 18 were used to improve event statistics as much as possible. The background situation for detector 175-4 (Fig. 26) is by far the worst and is thought to represent some kind of electronic problem and the fact that the data collection system did not distinguish events stopping in the last pulse-height-analyzed detector in the stack (the E'-detector in this case) from penetrating events. In Berkeley II penetrating events occurred in large numbers, due to a beam energy much higher than the optimum for these measurements. In this one case the situation was improved somewhat by imposing additional constraints on some of the earlier pulse heights in the stack, but the results obtained for this detector on the magnitude of the multiplication effect must necessarily be treated as upper limits. An enlarged version of Fig. 26, showing only the Z = 18 subset of the data used here, appears in Fig. 27.

A C program was written to calculate the probability of an event with given E' to be a bad event. This was a combination of the previously described program for calculating dE/dx, and a routine to do power-law interpolation in tables of bad event probability vs. dE/dx for each detector from Berkeley I (Tables III - VI). The program was run on the Berkeley II data for each 175-μm

ΔE_1-detector, taking each different bias run separately. Then the actual number of bad events was counted for each of these same cases. These two sets of values are tabulated for the four detectors in Tables VIII(a), IX, X, and XI(a). When the expected and actual numbers of bad events are compared, there is evidence of a definite bias-dependence to the effect, with biases lower than about 70% of full bias causing a significant reduction in the incidence of bad events. Unfortunately, the trend is obscured somewhat by the poor statistics and possible background effects. The situation can be made clearer by grouping together similar biases and also combining data for different detectors. Because detectors 175-1 and 175-4 were oriented opposite to the other two detectors in the stack, the data for these two were combined together, as were the data for the other pair, but the two orientations were not combined (the effect of reversing orientation will be discussed in Section V). The reduced data appears in Tables XII and XIII(a), and plotted in Fig. 28. From this data the bias-dependence is clear; for both detector orientations, a reduction to ~ 40% of the recommended bias results in reducing the occurrence of the multiplication effect by a factor of 6 - 7. This bias is rather close to depletion, however, so in practice a reduction to about half the recommended bias would probably be used, giving a reduction in bad events of about a factor of three.

V. DEPENDENCE ON DETECTOR ORIENTATION

In examining Tables VIII(a), IX, X and XI(a), it can be seen that the ratio of observed to predicted bad events is consistently lower for the two detectors which were reversed (aluminum side facing the beam) than for the other two. Moreover, the ratio in the high-bias runs is close to unity for the unreversed detectors, as expected, but is much less than unity for the reversed detectors. This pattern is of course retained when detectors of the same orientation are combined (Tables XII and XIII(a), Fig. 28). The pattern could be explained by recalling that the predictions are derived from Berkeley I data, in which all detectors had the gold side facing the beam, and that dE/dx was calculated at the back (aluminum) side of the ΔE_1-detector. If this surface is in fact the source of the multiplication effect, then predictions made using dE/dx at the back side of the detector will yield abnormally high results for reversed detectors, since bad event probability increases as a function of dE/dx and it is actually the much lower value of dE/dx at the *front* of the detector which is relevant in the reversed-orientation case. Thus the ratio of observed to predicted bad events would come out low, as is seen here. If this hypothesis is correct, then predictions made using Berkeley I data for probability vs. dE/dx, but calculating dE/dx at the front surface of the reversed ΔE_1-detector for each Berkeley II event, should yield results more like those already obtained for the unreversed detectors in Berkeley II, with observed/predicted ratios close to unity for the high-bias runs.

To test this, the program for calculating dE/dx was modified to give the value of dE/dx at the front instead of the back of the ΔE_1-detector; this change amounted to adding the ~175 μm of the detector itself in with the air gap. When the Berkeley II calculations for detectors 175-1 and 175-4 are repeated using dE/dx at the front of the detector, the bad observed/predicted ratio does indeed increase by a factor of 5 - 6, enough to make the ratio for the reversed detectors generally consistent with the unreversed detectors (Tables VIII(b), XI(b) and XIII(b), and Fig. 28). There may be background events (particularly in the data for detector 175-4) which have not been and cannot be completely accounted for; if this could be done it would tend to lower the reversed-detector curve slightly and perhaps give better agreement with the curve for the unreversed detectors. However, the effect of background removal would be expected to be concentrated at the lower biases where there are fewer bad events to begin with, rather than at full bias where the discrepancy is the greatest.

From these results one can conclude that while the aluminum surface of the detector is an important factor in generating the multiplication effect, more than this must probably be involved to explain the detector-reversal data. That the entire detector is involved is supported by the observation that the effect occurs only among particles that have passed completely through the detector, regardless of which side faces the beam. Good examples showing this exist in the Berkeley I data, but unfortunately only for the situation where the gold side faces the beam; the effect is exhibited by considering particles *stopping* in the surface-barrier detector under study and plotting their energy loss (E') against the energy loss in an earlier detector in the stack. Examples appear in Figs. 4 and 29, where the E'-detectors were detectors 500-3 and 175-4, respectively; the corresponding data for the other 175-μm detectors is similar. The only examples for the opposite orientation in the COMPAS detector data were obtained in Berkeley II and suffer from the poor statistics of that data. If one considers events stopping in the reversed 175-μm detectors and plots their energy loss (E') against the energy loss in a preceding 500-μm detector in the stack, the result is Figs. 30 and 31. (A 175-μm detector is not used as the ΔE-detector since this detector would show the effect also and to a comparable degree, making it difficult to identify instances of the effect in the E'-detector.) Despite the poor statistics and the fact that the 500-μm detectors do show the effect to a small degree, it is still possible to say that for this detector orientation, the multiplication effect for stopping events is at least an order of magnitude lower than it is for penetrating events in the same detector at comparable energy losses. In Figs. 29, 30 and 31, as in Fig. 4, bad events are seen only at the "fold-back" part of the element track, corresponding to particles which have actually passed through the "stopping" detector but had insufficient energy left to trigger the next detector in the stack. Better data (higher statistics and lower background) exists for the reversed-orientation situation in the HIST 150-μm detector Berkeley calibration data (Ref. 2); this shows no evidence for the multiplication effect in this detector with stopping events when the aluminum side faces the beam (see Appendix A).

If we assume for simplicity that the multiplication effect does occur on the aluminum surface of the detector, we can estimate the degree of improvement that would be achieved by reversing the detector's orientation in a cosmic ray instrument, so that the aluminum surface faces outward instead of inward. Reversing the detector has the effect of decreasing, by the thickness of the detector, the residual range at which the effect reaches a given magnitude. As noted earlier, lowering the bias voltage by about 50% gives a further reduction in bad event occurrence of about a factor of three (averaged over energy losses). If both steps are taken, the residual range at which the effect reaches a given severity is considerably reduced, as Fig. 32 demonstrates. The 2% and 30% bad event fraction contours of residual range vs. Z from Fig. 21 are presented, together with the new positions of the same bad event fraction contours if both bias voltage reduction and detector reversal are implemented. In this presentation (which is somewhat approximate) it is apparent that the 2% bad event level is now exceeded for Fe only in the first 800 μm of E'-detector, as compared with 2 mm previously. The 2% level is never reached at all for elements below Z = 16, and the 30% level is never reached for $Z < 31$. This is clearly a substantial improvement, and the possibilities of lower detector bias and optimum orientation warrant serious consideration in the design of future cosmic ray telescopes.

VI. SUMMARY AND POSSIBLE FUTURE WORK

To summarize what is currently known about the pulse height multiplication effect:

(1) It occurs most frequently in detectors with high field strengths (greater than ~6000 volts/cm).

(2) Its occurrence as a fraction of the total number of particles is an increasing function of dE/dx measured at the aluminum surface of the detector, with an apparent threshold near 4 - 5 GeV/(g/cm^2) for the particular detectors studied here.

(3) There is no evidence for the effect among particles that have not passed completely through the detector.

(4) The occurrence of the effect is considerably reduced (by a factor of ~6) by orienting the detector with the aluminum side facing outward rather than inward. This is a consequence of items (2) and (3) above. The reduction is by a factor of ~6 (averaged over energy) in this study, although the actual factor depends on the residual range (and hence initial energy) of the particle.

(5) The occurrence of the effect depends significantly on detector bias voltage, with a bias of ~50% of the recommended operating bias resulting in a reduction of about a factor of three in the incidence of bad events.

(6) There is no evidence for position-dependence of the effect over the surface of the detector, based on the position information included in the Berkeley I data. This makes it unlikely that the effect is caused by a localized irregularity or defect in the detector or its electrode surfaces.

(7) There is qualitative evidence for a dependence on particle incidence angle. This is derived from the HIST calibration data (Ref. 2, Appendix A), which was collected at incidence angles ranging 20° on either side of 0°. The dependence is not symmetrical about 0° and may be related in some way to the crystal structure of the silicon wafer.

(8) The "multiplication factor" (factor by which the pulse heights are increased) is variable between different detectors. This results from comparing multiplication effect data for different SRL detectors. The ~30% multiplication observed here is somewhat larger than that seen in the HIST and Voyager surface-barrier detectors.

Possible areas for further work on this subject are the following:

(1) Determine the quantitative dependence of the effect on detector field strength in different detectors. This would involve comparing the results obtained here with similar quantitative information obtained for the HIST and Voyager detectors showing the effect.

(2) Obtain a quantitative description of the incidence angle dependence, using the HIST calibration data.

(3) Extrapolate these results to other Z. The COMPAS data were obtained using only ^{40}Ar, but the HIST data includes both ^{40}Ar and ^{56}Fe nuclei, and lower charges are present in both cases due to fragmentation.

(4) Determine the change in the shape of the dE/dx dependence with bias or field strength. The bias-dependence of the effect determined here is only an average over values of dE/dx, on account of the poor Berkeley II statistics which precluded breaking down the data into energy bins. Limited results may still be possible with this data. Also, the HIST calibration data, although done only at nominal bias, involve different field strengths than the COMPAS 175-μm detectors and have good statistics. It would be useful to know whether the curves of bad event fraction vs. dE/dx (Fig. 20), if the bias were lowered, would simply shift down by a constant amount, raising the threshold, or retain the same threshold with a reduced slope.

(5) Determine the dependence of the "multiplication factor" on charge and on detector orientation. Both HIST and COMPAS data are applicable to this question.

(6) Develop a physical model for the effect. There are reports in the literature of pulse height multiplication-type effects (e.g., Ref. 5) but these involve lower energy particles (fission fragments) stopping in the detector, rather than penetrating particles. This effect may or may not be related to what has been observed here.

REFERENCES

(1) Cook, W. R., Ph.D. thesis, Appendix B.3, California Institute of Technology, Pasadena, California (1981).

(2) HIST Berkeley ^{40}Ar and ^{56}Fe calibration data (1976-78).

(3) Janni, J. F., "Calculations of Energy Loss, Range, Pathlength, Straggling, Multiple Scattering, and the Probability of Inelastic Nuclear Collisions for 0.1- to 1000-MeV Protons", Air Force Weapons Laboratory Technical Report No. AFWL-TR-65-150, Kirtland Air Force Base, New Mexico (1966).

(4) Barkas, W. H., and Berger, M. J., "Tables of Energy Losses and Ranges of Heavy Charged Particles", reprinted in "*Studies in Penetration of Charged Particles in Matter*", National Academy of Sciences/National Research Council publication 1133, Washington, D.C. (1964), p. 103.

(5) Walter, F. J., "Multiplication in the Fission Fragment Pulse Height Response of Silicon Surface Barriers", *IEEE Transactions on Nuclear Science*, June 1964, p. 232.

Table I. Characteristics of the eight Ortec surface barrier detectors involved in this study. Thickness, resistivity and recommended bias are supplied by Ortec; area and depletion voltage are measured in the laboratory at SRL.

SRL ID #	Ortec serial #	area (cm^2)	thickness (μm)	resistivity (KΩ-cm)	recommended operating bias (V)	depletion voltage[1]	p- or n-type silicon
175-1	20-126B	19.46	166.4	1.73	100	50	p
175-2	20-300D	19.59	175.4	1.73	125	63	p
175-3	20-332C	18.95	160.2	1.33	125	40	p
175-4	20-470B	19.37	161.2	1.47	125	36	p
500-1	20-066A	19.67	476.2	30 ?	150	~40	n
500-2	20-598D	19.67	508.0	15.1	200	~90	n
500-3	20-613A	19.31	452.8	24	150	~90	p
500-5	20-598A	19.76	505.6	15.1	250	75-100	n

[1] Depletion voltage is defined as the bias voltage at which the measured energy loss of a stopping α-particle is 0.1% less than that measured at the recommended operating bias.

Table II. Bias voltages of all detectors in the ten Bevalac runs used in this report. Biases in Berkeley I are the manufacturer's recommended operating biases for the respective detectors.

Berkeley I, stack 13, run 39		Berkeley I, stack 18, run 47	
detector SRL ID #	bias voltage	detector SRL ID #	bias voltage
M2	37	M3	37
M10	37	3-9	500
M5	37	175-1	100
M9	37	3-10	500
175-2	125	175-3	125
500-3	150	3-11	500
1.7-2	300	175-4	125
3-11	500	3-12	500
3-12	500	3-1	500

detector	bias voltage for Berkeley II run #:							
SRL ID #	1	2	3	4	5	6	7	8
500-5	250	250	250	150	200	250	100	125
175-1	55	55	100	75	63	55	85	50
175-2	125	125	69	95	79	125	110	63
500-2	200	100	100	125	150	200	175	100
175-3	44	44	60	85	125	44	50	105
175-4	40	40	80	125	54	40	65	100
3-6	500	500	500	500	500	500	500	500
3-7	500	500	500	500	500	500	500	500

Table III. Berkeley I data on dE/dx-dependence of the multiplication effect in ΔE_1-detector 175-1 (Z = 18 only). dE/dx is calculated at the back (aluminum) surface of the ΔE_1-detector.

E' interval (MeV)	bad events	total events	fraction bad	dE/dx interval (GeV/(g/cm²))	<E'> (MeV)	<dE/dx> (GeV/(g/cm²))
42.4 - 118.6	25	28	$.893^{+.058}_{-.093}$	16.16 - 18.78	79.6	17.56
118.6 - 228.8	20	38	$.526^{+.092}_{-.094}$	12.89 - 16.16	175.7	14.31
228.8 - 339.0	28	81	$.346^{+.061}_{-.056}$	10.66 - 12.89	289.8	11.56
339.0 - 457.6	28	104	$.269^{+.051}_{-.046}$	8.95 - 10.66	405.9	9.61
457.6 - 576.3	22	147	$.150^{+.035}_{-.030}$	7.72 - 8.95	521.4	8.24
576.3 - 678.0	15	157	$.095^{+.030}_{-.024}$	6.93 - 7.72	625.0	7.33
678.0 - 779.7	9	151	$.060^{+.026}_{-.019}$	6.29 - 6.93	731.2	6.58
779.7 - 881.4	5	147	$.0340^{+.0224}_{-.0146}$	5.77 - 6.29	831.1	6.01
881.4 - 974.6	2	134	$.0149^{+.0194}_{-.0096}$	5.36 - 5.77	922.3	5.58
974.6 - 1076.	2	133	$.0150^{+.0195}_{-.0097}$	4.99 - 5.36	1020.	5.19
1076. - 1415.	2	383	$.0052^{+.0069}_{-.0034}$	4.14 - 4.99	1241.	4.51
1415. - 2653.	1	2390	$.00042^{+.00096}_{-.00035}$	2.56 - 4.14	2059.	3.11
2653. - 3000.	0	1215	$.0000^{+.0015}_{-.0000}$	2.34 - 2.56	2806.	2.46

Table IV. Berkeley I data on dE/dx-dependence of the multiplication effect in ΔE_1-detector 175-2 (Z = 18 only). dE/dx is calculated at the back (aluminum) surface of the ΔE_1-detector.

E' interval (MeV)	bad events	total events	fraction bad	dE/dx interval (GeV/(g/cm²))	<E'> (MeV)	<dE/dx> (GeV/(g/cm²))
5 - 75	87	108	$.806^{+.039}_{-.046}$	17.74 - 19.73	40.2	18.89
75 - 130	79	100	$.790^{+.042}_{-.049}$	15.77 - 17.74	102.6	16.72
130 - 195	105	159	$.660^{+.039}_{-.042}$	13.80 - 15.77	163.0	14.72
195 - 265	122	219	$.557^{+.035}_{-.036}$	12.08 - 13.80	229.7	12.88
265 - 340	102	262	$.389^{+.032}_{-.031}$	10.66 - 12.08	302.5	11.32
340 - 415	95	344	$.276^{+.026}_{-.025}$	9.49 - 10.66	378.4	10.01
415 - 490	96	451	$.213^{+.021}_{-.020}$	8.59 - 9.49	455.7	8.97
490 - 570	114	635	$.180^{+.017}_{-.015}$	7.78 - 8.59	532.7	8.13
570 - 645	84	725	$.116^{+.013}_{-.012}$	7.17 - 7.78	609.1	7.45
645 - 710	71	873	.081 ± .009	6.72 - 7.17	678.7	6.93
710 - 770	71	1057	.067 ± .008	6.35 - 6.72	740.7	6.52
770 - 830	61	1226	.050 ± .006	6.02 - 6.35	800.9	6.17
830 - 885	56	1345	.042 ± .005	5.75 - 6.02	858.2	5.88
885 - 925	23	1383	.017 ± .003	5.57 - 5.75	905.8	5.66
925 - 970	34	1516	.022 ± .004	5.38 - 5.57	945.2	5.49
970 - 995	1	58	$.017^{+.039}_{-.014}$	5.29 - 5.38	975.9	5.36

Table V. Berkeley I data on dE/dx-dependence of the multiplication effect in ΔE_1-detector 175-3 (Z = 18 only). dE/dx is calculated at the back (aluminum) surface of the ΔE_1-detector.

E' interval (MeV)	bad events	total events	fraction bad	dE/dx interval (GeV/(g/cm^2))	<E'> (MeV)	<dE/dx> (GeV/(g/cm^2))
10 - 120	19	23	$.826\,^{+.081}_{-.116}$	16.11 - 19.63	63.3	18.13
120 - 240	19	30	$.633\,^{+.098}_{-.108}$	12.62 - 16.11	180.0	14.19
240 - 380	15	46	$.326\,^{+.083}_{-.075}$	9.98 - 12.62	317.0	11.02
380 - 500	3	47	$.064\,^{+.058}_{-.035}$	8.47 - 9.98	435.4	9.21
500 - 640	4	71	$.056\,^{+.042}_{-.027}$	7.21 - 8.47	569.2	7.78
640 - 760	3	85	$.035\,^{+.033}_{-.019}$	6.40 - 7.21	707.5	6.73
760 - 880	4	129	$.031\,^{+.024}_{-.015}$	5.77 - 6.40	832.1	6.01
880 - 970	2	129	$.016\,^{+.020}_{-.010}$	5.38 - 5.77	928.9	5.55
970 - 1170	1	493	$.0020\,^{+.0047}_{-.0016}$	4.70 - 5.38	1076.	4.99
1170 - 3000	0	6483	$.00000\,^{+.00029}_{-.00000}$	2.34 - 4.70	2337.	2.83

Table VI. Berkeley I data on dE/dx-dependence of the multiplication effect in ΔE_1-detector 175-4 (Z = 18 only). dE/dx is calculated at the back (aluminum) surface of the ΔE_1-detector.

E' interval (MeV)	bad events	total events	fraction bad	dE/dx interval (GeV/(g/cm²))	<E'> (MeV)	<dE/dx> (GeV/(g/cm²))
10 - 190	98	99	$.990^{+.008}_{-.023}$	13.92 - 19.63	125.0	15.92
190 - 250	55	56	$.982^{+.015}_{-.040}$	12.39 - 13.92	222.0	13.07
250 - 300	48	49	$.980^{+.017}_{-.045}$	11.36 - 12.39	279.3	11.77
300 - 420	65	105	$.619^{+.051}_{-.053}$	9.41 - 11.36	356.4	10.36
420 - 540	64	177	$.362^{+.040}_{-.038}$	8.05 - 9.41	484.3	8.65
540 - 660	37	233	$.159^{+.028}_{-.025}$	7.06 - 8.05	601.4	7.51
660 - 770	19	256	$.074^{+.020}_{-.017}$	6.34 - 7.06	720.0	6.65
770 - 850	10	307	$.0326^{+.0135}_{-.0101}$	5.92 - 6.34	810.2	6.12
850 - 920	4	265	$.0151^{+.0118}_{-.0072}$	5.59 - 5.92	884.6	5.75
920 - 1000	1	335	$.0030^{+.0068}_{-.0025}$	5.27 - 5.59	962.1	5.41
1000 - 1060	2	252	$.0079^{+.0104}_{-.0051}$	5.05 - 5.27	1031.	5.15
1060 - 1120	1	226	$.0044^{+.0101}_{-.0036}$	4.85 - 5.05	1089.	4.95
1120 - 1220	1	360	$.0028^{+.0063}_{-.0023}$	4.56 - 4.85	1169.	4.70
1220 - 1290	1	243	$.0041^{+.0094}_{-.0034}$	4.39 - 4.56	1256.	4.47
1290 - 1460	1	676	$.00148^{+.00339}_{-.00122}$	4.06 - 4.39	1379.	4.21
1460 - 1800	1	2076	$.00048^{+.00111}_{-.00040}$	3.46 - 4.06	1621.	3.75
1800 - 2170	1	1418	$.00071^{+.00161}_{-.00059}$	2.99 - 3.46	1971.	3.22
2170 - 2520	1	856	$.00117^{+.00268}_{-.00097}$	2.67 - 2.99	2339.	2.83
2520 - 2970	0	587	$.0000^{+.0031}_{-.0000}$	2.36 - 2.67	2710.	2.52

Table VII. Berkeley I data on dE/dx-dependence of the multiplication effect in ΔE_1-detector 500-3 (Z = 18 only). dE/dx is calculated at the back (aluminum) surface of the ΔE_1-detector.

E' interval (MeV)	bad events	total events	fraction bad	dE/dx interval (GeV/(g/cm²))	<E'> (MeV)	<dE/dx> (GeV/(g/cm²))
30 - 100	23	272	$.085\ ^{+.020}_{-.017}$	16.75 - 19.12	74.2	17.71
100 - 160	24	377	$.064\ ^{+.015}_{-.013}$	14.78 - 16.75	130.2	15.72
160 - 220	25	469	$.053\ ^{+.013}_{-.010}$	13.11 - 14.78	190.8	13.89
220 - 350	25	1122	.0223 ± .0044	10.47 - 13.11	286.5	11.62
350 - 740	26	3247	.0080 ± .0016	6.52 - 10.47	541.1	8.04

Table VIII. Berkeley II data on dE/dx-dependence of the multiplication effect in ΔE_1-detector 175-1 (Z = 18 only).

(a) dE/dx used by the prediction program was calculated at the back (gold) surface of the ΔE_1-detector.

ΔE_1-detector bias (V)	percent of recommended bias	observed bad	observed total	observed fraction bad	predicted bad	predicted fraction bad	ratio of bad observed to bad predicted
100	100	5	31	$.161^{+.094}_{-.068}$	13.5	.435±.034	$.370^{+.218}_{-.159}$
85	85	4	34	$.118^{+.083}_{-.055}$	17.3	.509±.040	$.231^{+.164}_{-.110}$
75	75	1	10	$.100^{+.194}_{-.083}$	4.5	.450±.036	$.222^{+.431}_{-.185}$
63	63	1	14	$.071^{+.146}_{-.059}$	5.8	.414±.033	$.172^{+.352}_{-.143}$
55	55	5	92	$.054^{+.035}_{-.023}$	40.2	.437±.035	$.124^{+.081}_{-.054}$
50	50	1	19	$.053^{+.111}_{-.044}$	8.3	.437±.035	$.120^{+.254}_{-.101}$

(b) dE/dx used by the prediction program was calculated at the front (aluminum) surface of the ΔE_1-detector.

predicted bad	predicted fraction bad	ratio of bad observed to bad predicted
2.9	.094±.007	$1.72^{+1.01}_{-0.74}$
3.5	.103±.008	$1.14^{+0.81}_{-0.54}$
1.0	.100±.008	$1.00^{+1.94}_{-0.83}$
1.4	.100±.008	$.714^{+1.46}_{-.594}$
8.5	.092±.007	$.588^{+.382}_{-.253}$
1.8	.095±.008	$.556^{+1.17}_{-.467}$

Table IX. Berkeley II data on bias-dependence of the multiplication effect in ΔE_1-detector 175-2 (Z = 14 through 18 summed). dE/dx used by the prediction program is calculated at the back (aluminum) surface of the ΔE_1-detector.

ΔE_1-detector bias (V)	percent of recommended bias	observed bad	observed total	observed fraction bad	predicted bad	predicted fraction bad	ratio of bad observed to bad predicted
125	100	94	530	$.177^{+.018}_{-.017}$	86.4	.163 ±.005	$1.09^{+0.12}_{-0.11}$
110	88	45	269	$.167^{+.028}_{-.023}$	42.3	.157 ±.005	$1.06^{+0.17}_{-0.16}$
95	76	14	72	$.194^{+.058}_{-.048}$	13.5	.188 ±.005	$1.04^{+0.31}_{-0.26}$
79	63.2	9	56	$.161^{+.085}_{-.051}$	11.1	.198 ±.006	$.811^{+.328}_{-.258}$
69	55.2	15	170	$.088^{+.027}_{-.022}$	27.0	.159 ±.005	$.556^{+.171}_{-.140}$
63	50.4	10	192	$.052^{+.021}_{-.016}$	28.8	.150 ±.004	$.347^{+.140}_{-.107}$

Table X. Berkeley II data on bias-dependence of the multiplication effect in ΔE_1-detector 175-3 (Z = 18 only). dE/dx used by the prediction program is calculated at the back (aluminum) surface of the ΔE_1-detector.

ΔE_1-detector bias (V)	percent of recommended bias	observed bad	observed total	observed fraction bad	predicted bad	predicted fraction bad	ratio of bad observed to bad predicted
125	100	3	16	$.188^{+.149}_{-.100}$	4.3	.269 ±.032	$.698^{+.559}_{-.381}$
105	84	6	23	$.261^{+.123}_{-.098}$	8.3	.361 ±.043	$.723^{+.352}_{-.286}$
85	68	4	16	$.250^{+.154}_{-.115}$	6.7	.419 ±.050	$.597^{+.375}_{-.284}$
60	48	1	10	$.100^{+.194}_{-.083}$	4.2	.420 ±.050	$.238^{+.463}_{-.200}$
50	40	3	51	$.059^{+.054}_{-.032}$	20.6	.404 ±.048	$.146^{+.135}_{-.081}$
44	35.2	4	73	$.055^{+.041}_{-.026}$	26.8	.367 ±.044	$.149^{+.112}_{-.073}$

Table XI. Berkeley II data on bias-dependence of the multiplication effect in ΔE_1-detector 175-4 (Z = 18 only).

(a) dE/dx used by the prediction program was calculated at the back (gold) surface of the ΔE_1-detector.

ΔE_1-detector bias (V)	percent of recommended bias	observed bad	observed total	observed fraction bad	predicted bad	predicted fraction bad	ratio of bad observed to bad predicted
125	100	6	60	$.100^{+.055}_{-.039}$	19.8	.330±.016	$.303^{+.167}_{-.119}$
100	80	2	65	$.031^{+.039}_{-.020}$	21.6	.332±.017	$.093^{+.117}_{-.060}$
80	64	0	37	$.000^{+.049}_{-.000}$	11.8	.319±.016	$.000^{+.148}_{-.000}$
65	52	3	147	$.020^{+.019}_{-.011}$	57.4	.390±.019	$.052^{+.049}_{-.028}$
54	43.2	0	64	$.000^{+.028}_{-.000}$	17.6	.275±.014	$.000^{+.102}_{-.000}$
40	32	2	207	$.0097^{+.0128}_{-.0063}$	64.8	.313±.016	$.031^{+.040}_{-.020}$

(b) dE/dx used by the prediction program was calculated at the front (aluminum) surface of the ΔE_1-detector.

predicted bad	predicted fraction bad	ratio of bad observed to bad predicted
3.1	.052±.003	$1.94^{+1.07}_{-0.76}$
3.6	.055±.003	$.556^{+.705}_{-.362}$
2.1	.057±.003	$.000^{+.860}_{-.000}$
10.0	.068±.003	$.300^{+.280}_{-.162}$
2.7	.042±.002	$.000^{+.867}_{-.000}$
10.5	.051±.003	$.190^{+.249}_{-.125}$

Table XII. Berkeley II data on bias-dependence of the multiplication effect in ΔE_1-detectors 175-2 and 175-3. The data in Tables IX and X have been combined, and similar biases have also been combined. dE/dx used by the prediction program was calculated at the back (aluminum) surface of the ΔE_1-detector.

average percent bias	observed bad	observed total	observed fraction bad	predicted bad	predicted fraction bad	ratio of bad observed to bad predicted
100.0	60	302	$.199^{+.026}_{-.023}$	62.3	$.206\pm.007$	$.963^{+.130}_{-.116}$
87.5	41	193	$.212^{+.034}_{-.030}$	40.1	$.208\pm.008$	$1.022^{+.169}_{-.150}$
69.9	22	110	$.200^{+.046}_{-.040}$	26.9	$.245\pm.010$	$.818^{+.191}_{-.167}$
52.7	14	180	$.078^{+.025}_{-.020}$	37.2	$.207\pm.007$	$.376^{+.123}_{-.098}$
37.2	7	124	$.057^{+.029}_{-.021}$	47.4	$.382\pm.046$	$.148^{+.078}_{-.057}$

Table XIII. Berkeley II data on bias-dependence of the multiplication effect in ΔE_1-detectors 175-1 and 175-4. Data in Tables VIII and XI have been combined, and similar biases have also been combined.

(a) dE/dx used by the prediction program was calculated at the back (gold) surface of the ΔE_1-detector.

average percent bias	observed bad	observed total	observed fraction bad	predicted bad	predicted fraction bad	ratio of bad observed to bad predicted
100.0	11	91	$.121^{+.044}_{-.035}$	33.3	$.366\pm.022$	$.330^{+.122}_{-.098}$
81.1	7	109	$.064^{+.033}_{-.023}$	43.4	$.398\pm.025$	$.161^{+.083}_{-.059}$
63.7	1	51	$.020^{+.044}_{-.016}$	17.6	$.345\pm.020$	$.057^{+.128}_{-.046}$
52.9	9	258	$.035^{+.016}_{-.011}$	105.9	$.410\pm.026$	$.085^{+.039}_{-.027}$
34.6	2	271	$.0074^{+.0096}_{-.0048}$	82.4	$.304\pm.015$	$.024^{+.032}_{-.016}$

(b) dE/dx used by the prediction program was calculated at the front (aluminum) surface of the ΔE_1-detector.

predicted bad	predicted fraction bad	ratio of bad observed to bad predicted
6.0	$.066\pm.004$	$1.83^{+0.68}_{-0.54}$
8.1	$.074\pm.005$	$.864^{+.447}_{-.314}$
3.5	$.069\pm.004$	$.286^{+.641}_{-.234}$
20.3	$.079\pm.005$	$.443^{+.205}_{-.143}$
13.2	$.049\pm.002$	$.152^{+.197}_{-.099}$

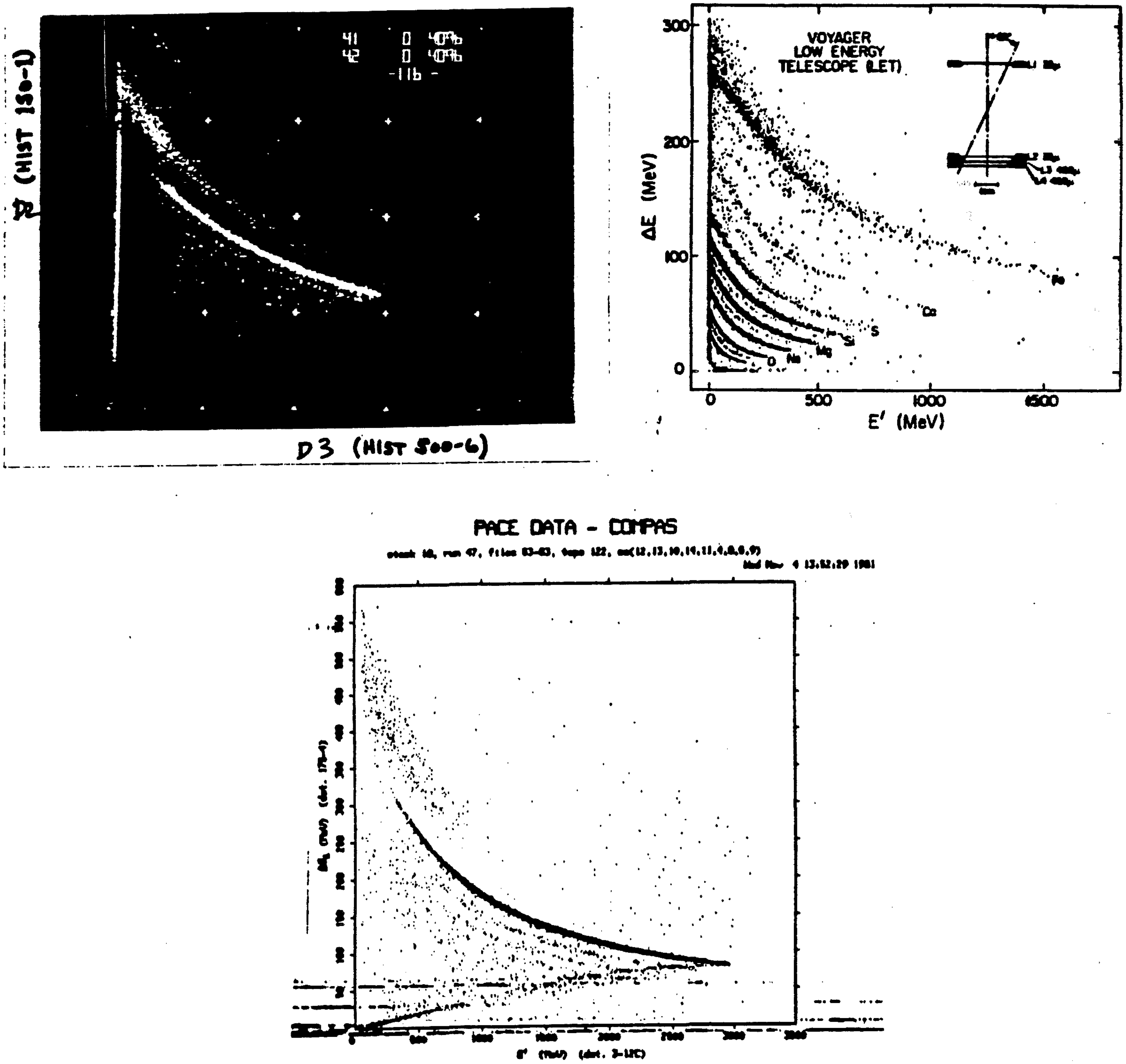

Fig. 1. Examples of ΔE_1-E' plots for various SRL surface-barrier detectors showing the multiplication effect. Included are HIST 150-μm detector Berkeley calibration data (top left), Voyager LET 35-μm detector flight data (top right), and COMPAS 175-μm detector Berkeley calibration data (bottom).

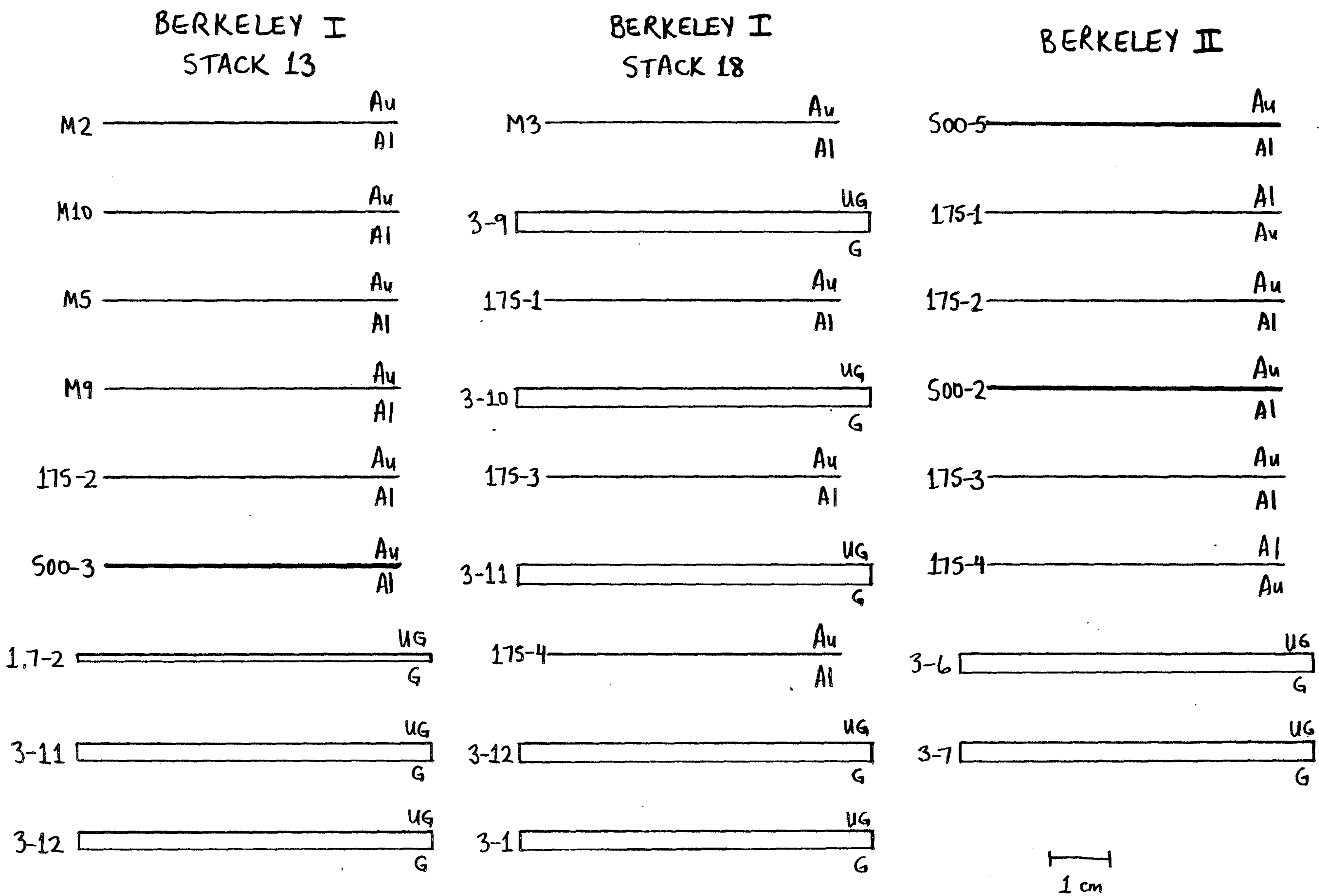

Fig. 2. Diagrams (to scale) of the three Berkeley calibration detector stacks used in analyzing the multiplication effect. In each case all detectors are mounted at an angle of 5° to the direction of the beam, which is incident from the top of the figure. "Au" and "Al" denote the gold- and aluminum-coated sides of the surface-barrier detectors; "G" and "UG" denote the grooved and ungrooved sides of the 1.7- and 3-mm lithium-drifted detectors.

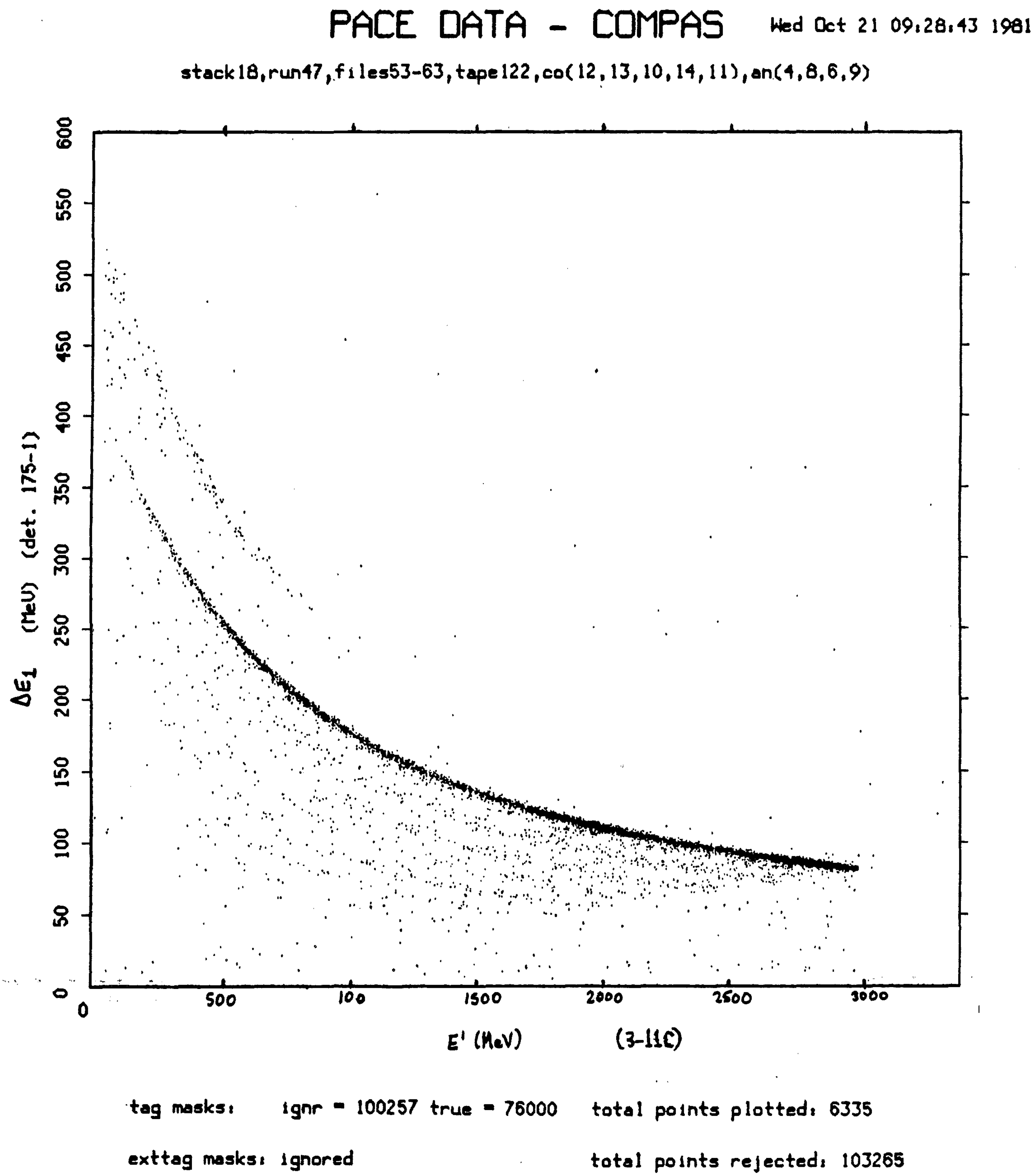

Fig. 3. Scatter-plot of ΔE_1 (detector 175-1) vs. E' (detector 3-11C) from Berkeley I. The track of particles above the main Z = 18 track are those showing the multiplication effect in the ΔE_1 detector.

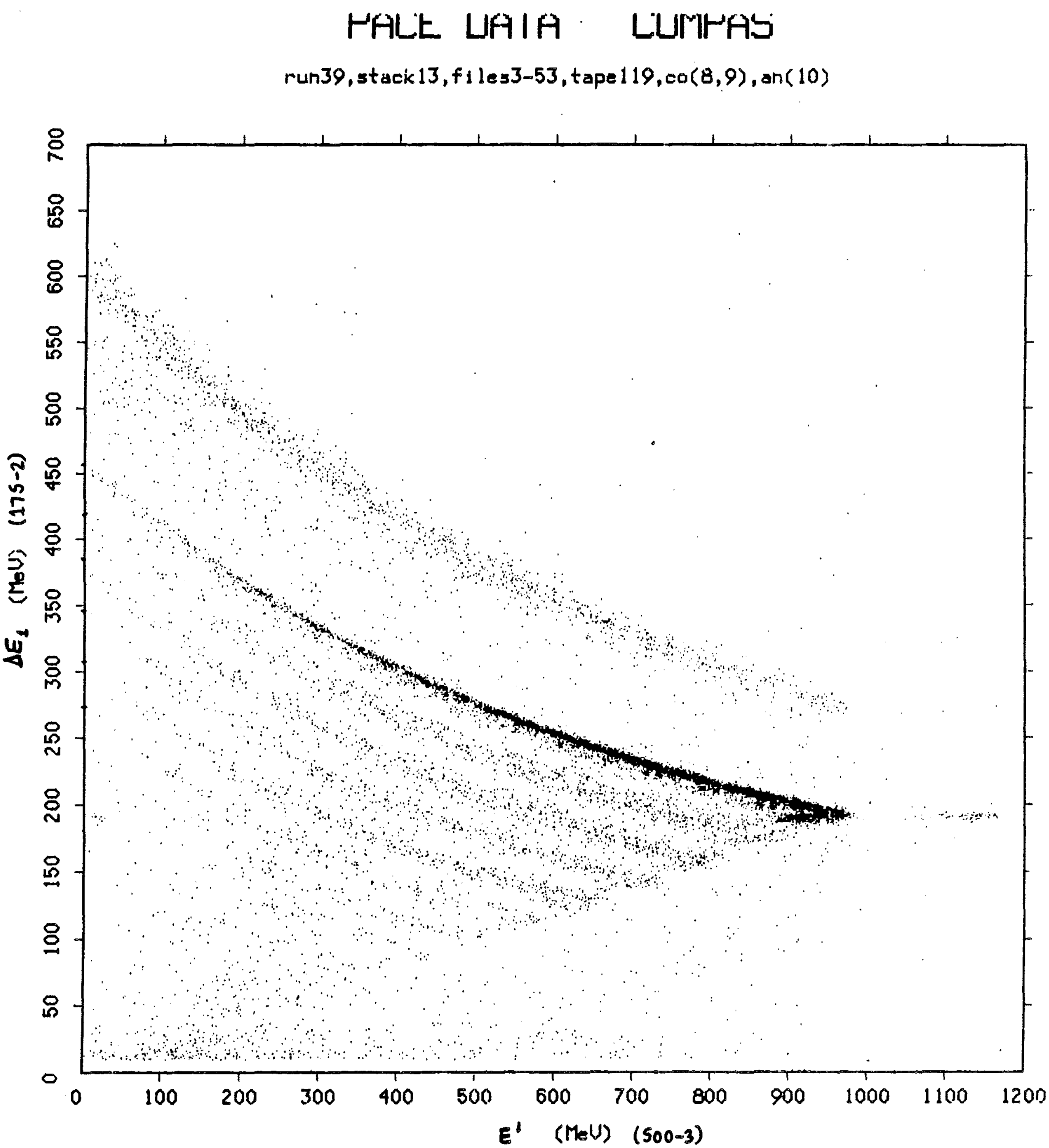

Fig. 4. Scatter-plot of ΔE_1 (detector 175-2) vs. E' (detector 500-3) from Berkeley I. The track running 100 - 150 MeV above the main Z = 18 track consists of Z = 18 events showing the multiplication effect in the 175-μm detector. The small cluster of points at the far right side displays the multiplication effect in the 500-μm detector. This is evidence that the effect occurs only when the particles have passed completely through a detector when the gold side is facing the beam. Here bad events are seen to the right of only the "fold-back" part of the argon track, corresponding to particles which have penetrated the 500-μm detector but were left with a residual energy below the triggering threshold of the next detector in the stack.

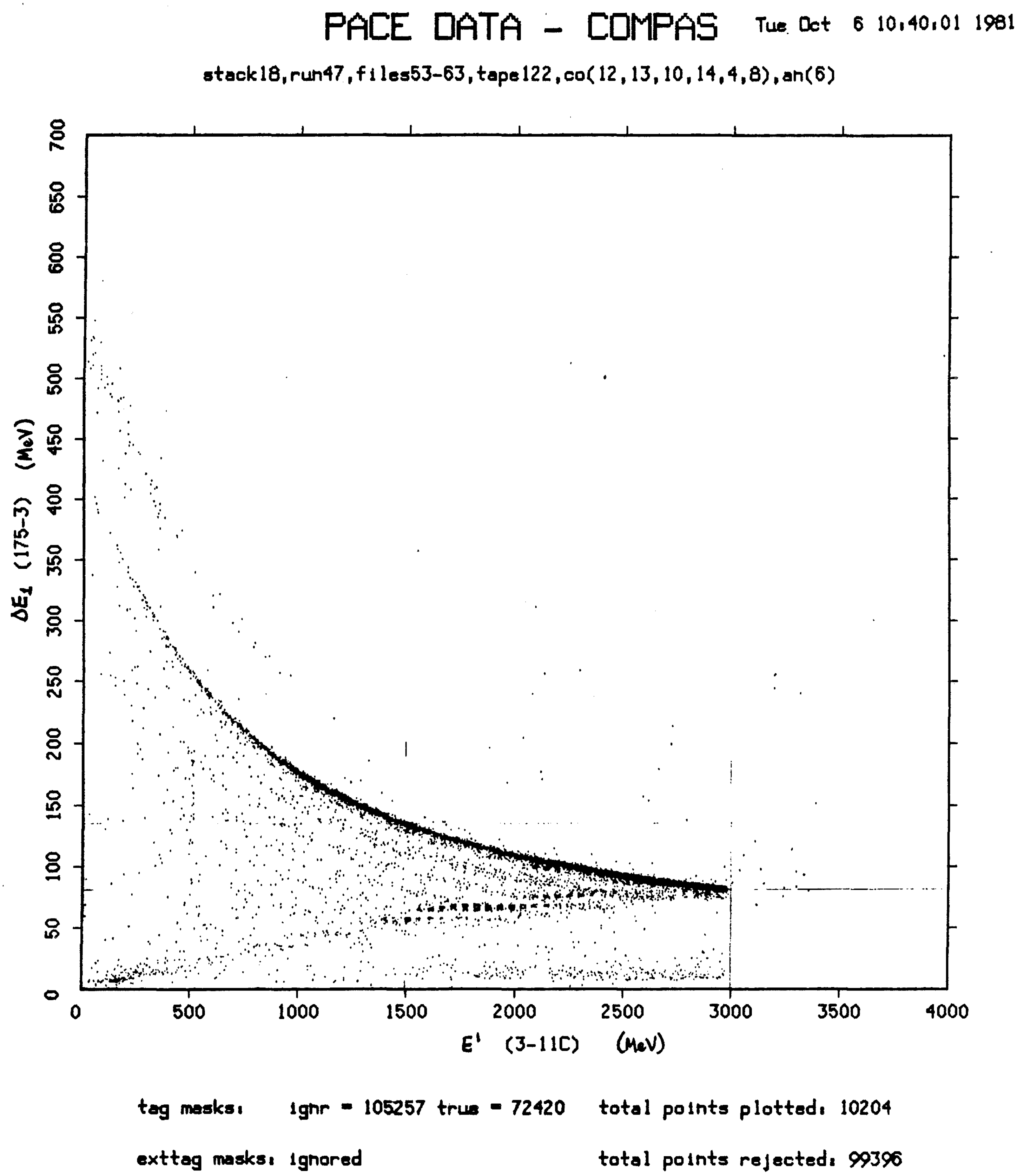

Fig. 5. Scatter-plot of ΔE_1 (detector 175-3) vs. E′ (detector 3-11C) from Berkeley I. The track of particles above the main Z = 18 track are those showing the multiplication effect in the ΔE_1 detector.

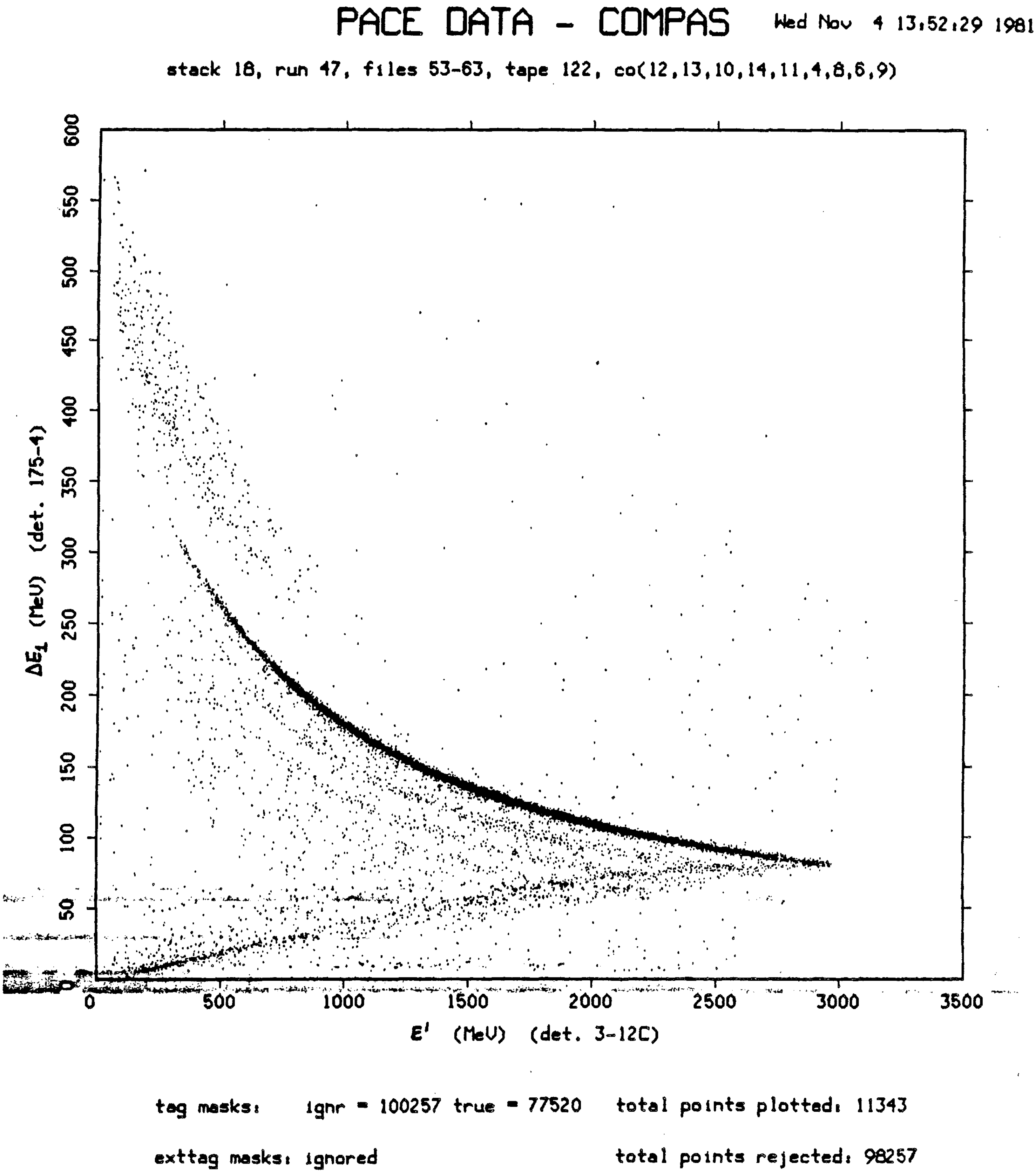

Fig. 6. Scatter-plot of ΔE_1 (detector 175-4) vs. E' (detector 3-12C) from Berkeley I. Unlike the other detectors tested, this one shows a "double-valued" multiplication effect forming two parallel tracks.

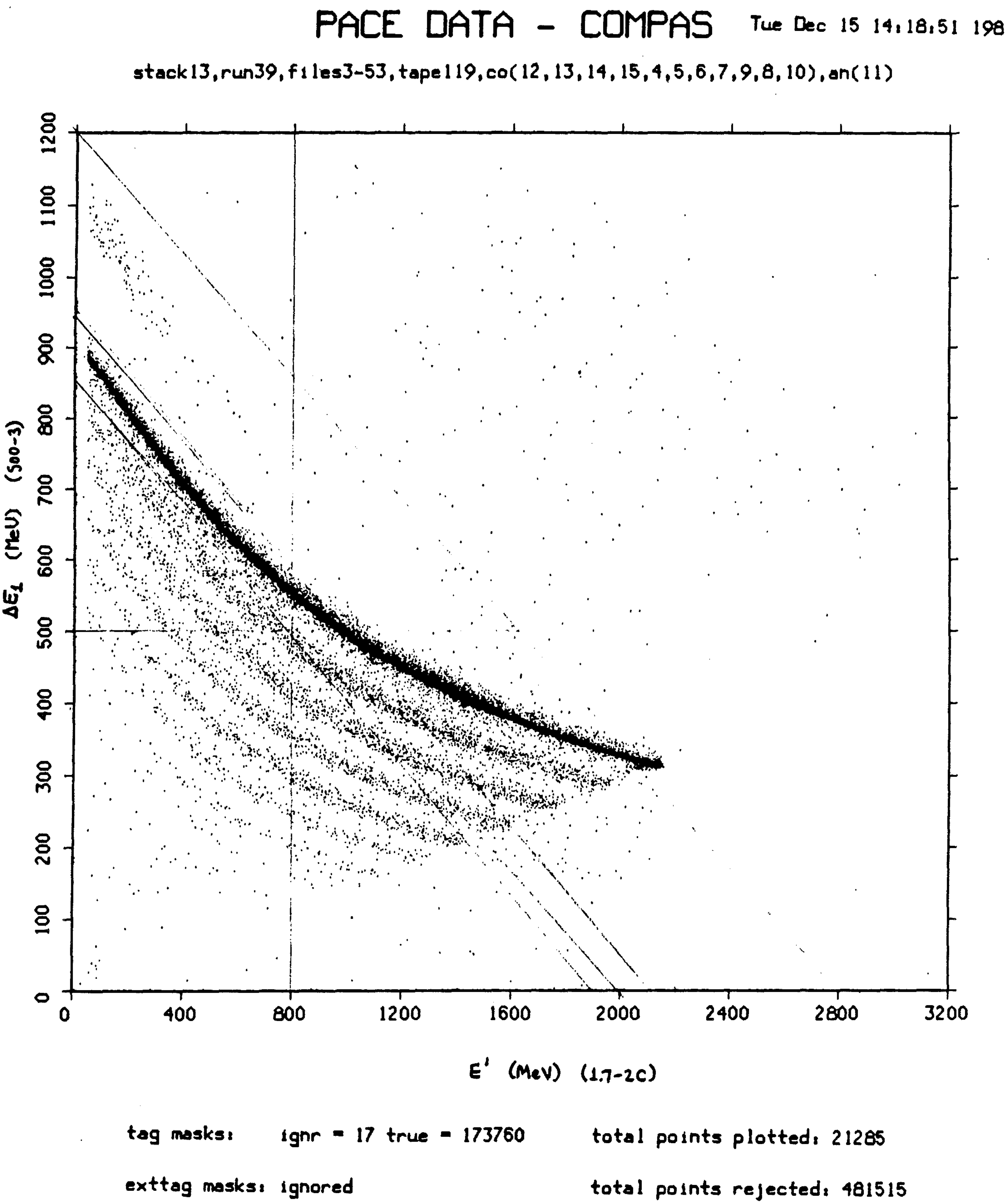

Fig. 7. Scatter-plot of ΔE_1 (detector 500-3) vs. E' (detector 1.7-2C) from Berkeley I. The track of particles above the main Z = 18 track are those showing the multiplication effect in the ΔE_1 detector.

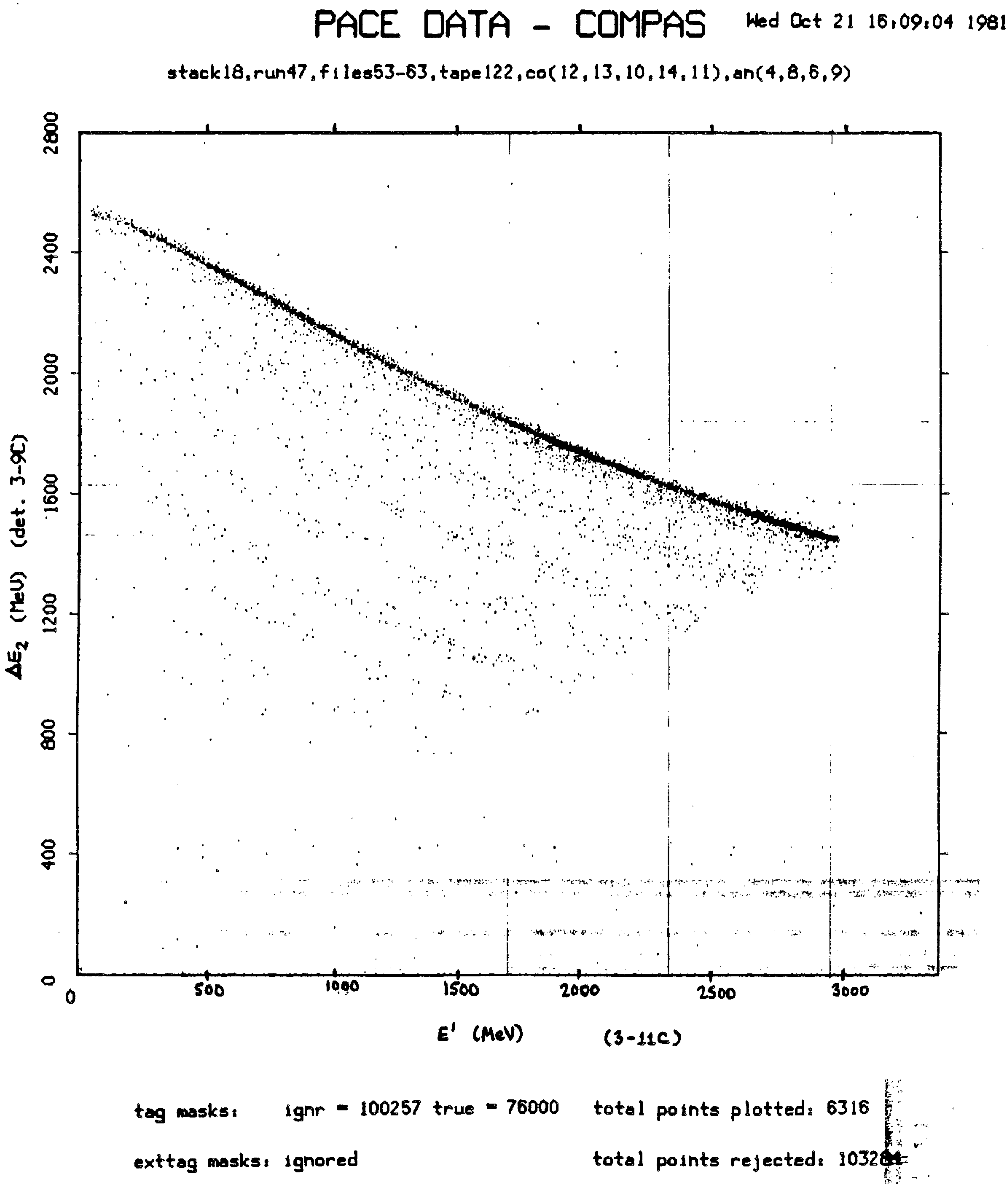

Fig. 8. Scatter-plot of ΔE_2 (detector 3-9C) vs. E' (detector 3-11C) from Berkeley I. No "bad" events are apparent, since only the ΔE_1 pulse height is in error.

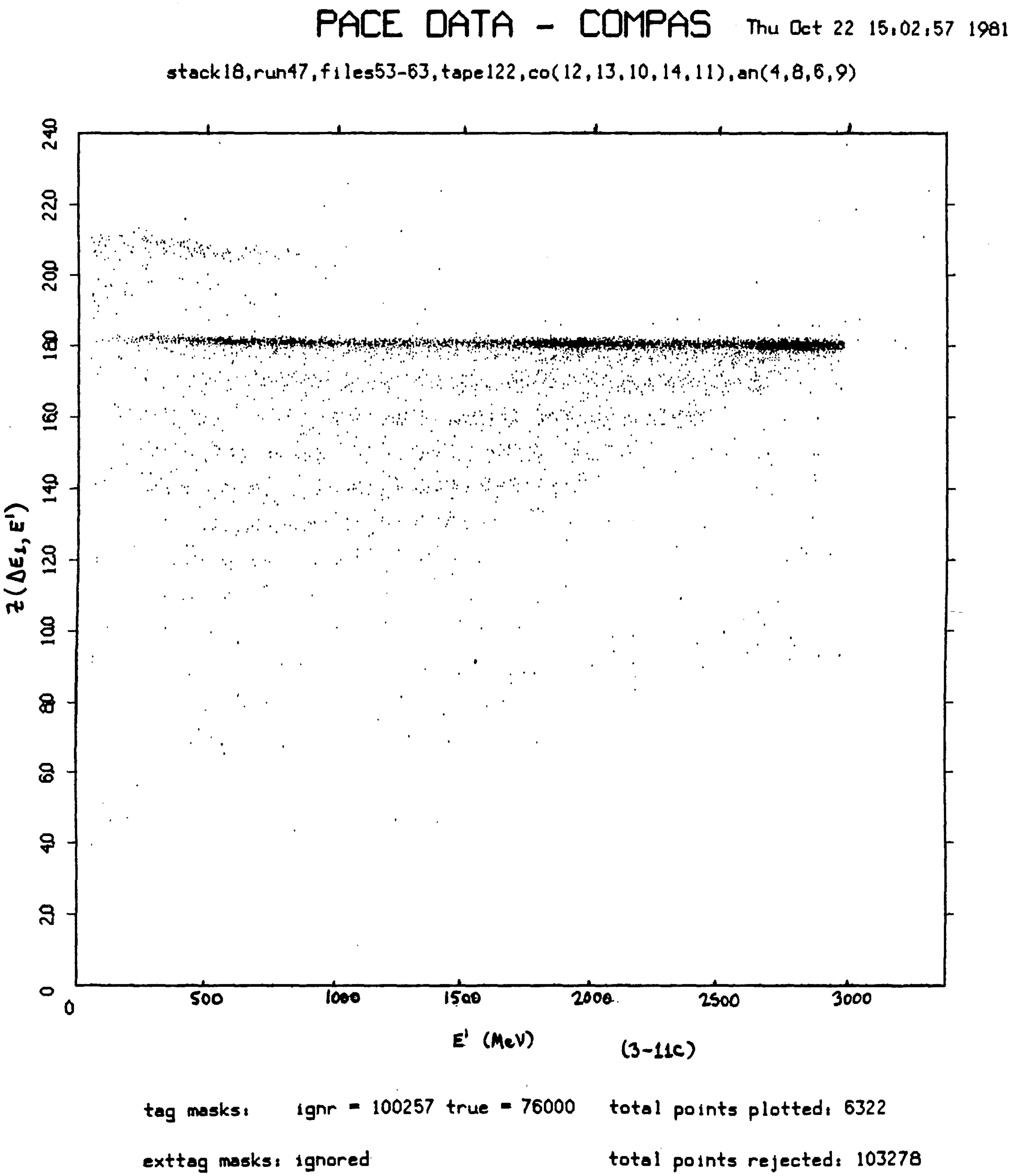

Fig. 9. Scatter-plot of $Z(\Delta E_1, E')$ vs. E' (detector 3-11C). This plot is derived from the data in Fig. 3. Note how the erroneous ΔE_1 pulse height affects this calculation of Z for the "bad" events.

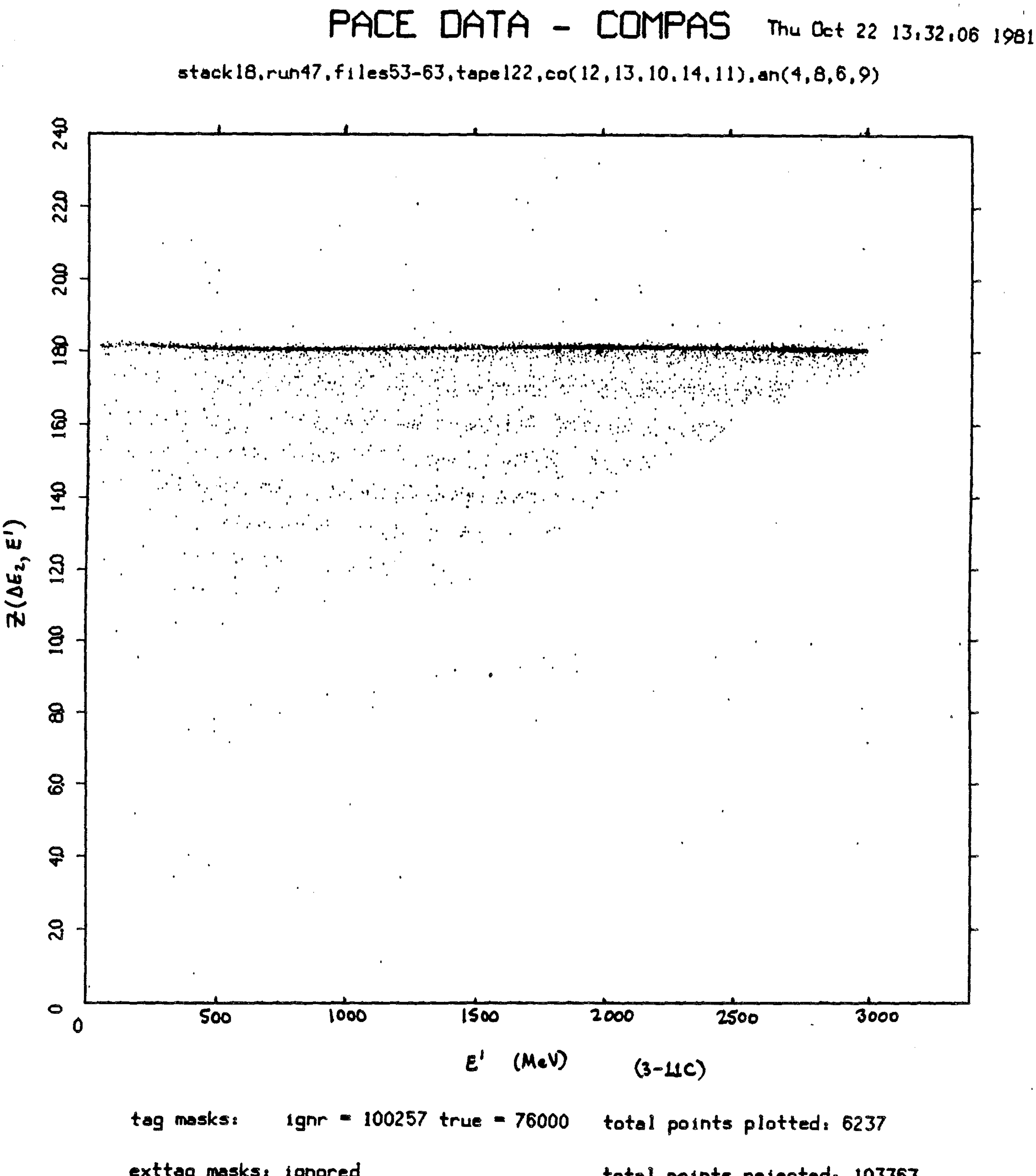

Fig. 10. Scatter-plot of $Z(\Delta E_2, E')$ vs. E' (detector 3-11C). This plot is derived from the data in Fig. 8. Note that no "bad" events are apparent, since the erroneous ΔE_1 pulse height is not involved in this determination of Z. There is a small amount of background in the same region of this plot (and in the others of this series) caused by such factors as "pileup" (more than one particle arriving at the same time, giving a larger energy loss than a single particle) and nuclear reactions of beam particles in detectors or absorbers (for instance, Z = 19 can be formed by the reaction $^{40}Ar + p \rightarrow {}^{40}K + n$).

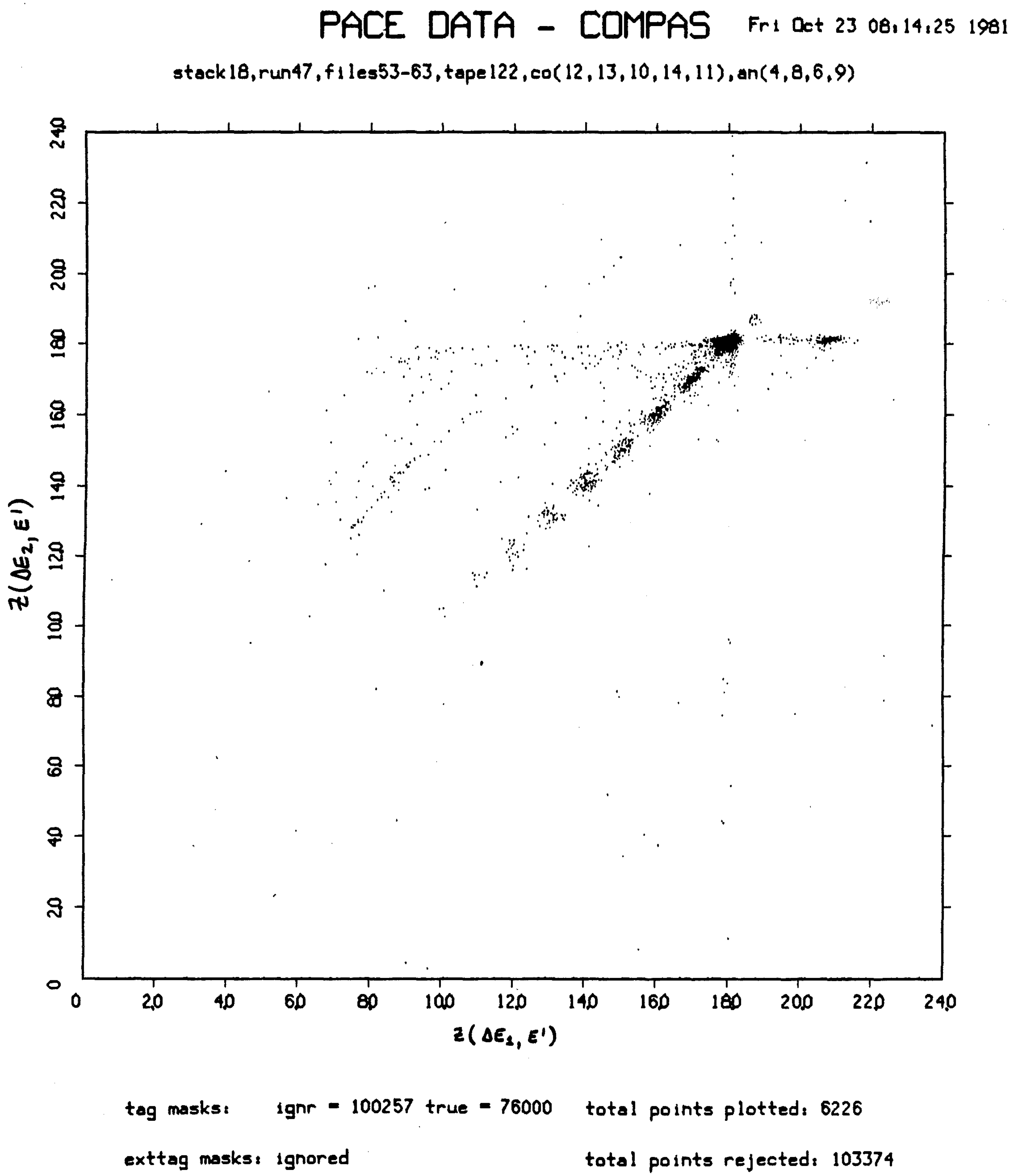

Fig. 11. Cross-plot of Z(ΔE_2,E') vs. Z(ΔE_1,E') from Berkeley I, separating the "good" events from those with anomalously high pulse height in the ΔE_1-detector, 175-1.

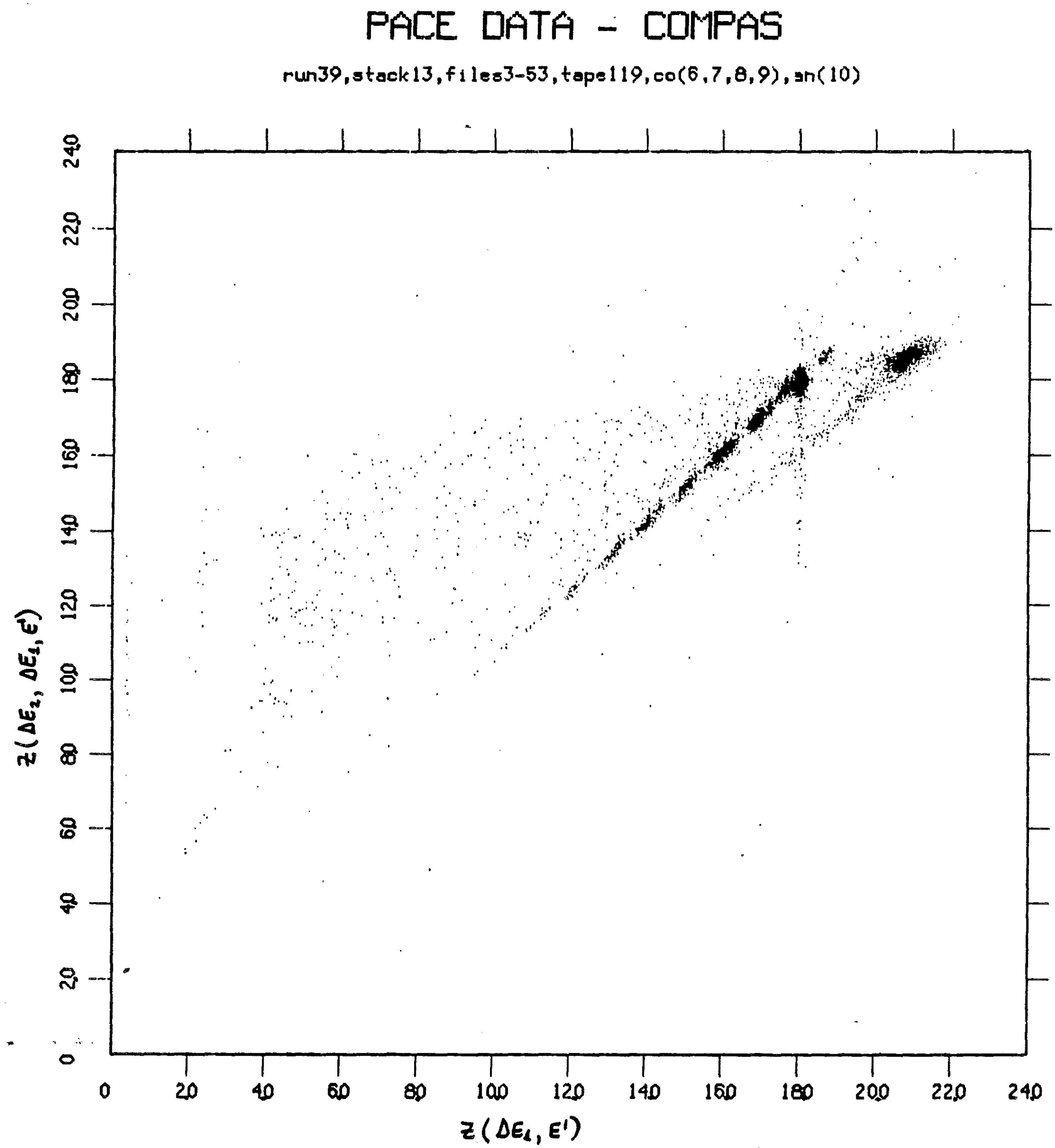

Fig. 12. Cross-plot of $Z(\Delta E_2, \Delta E_1, E')$ vs. $Z(\Delta E_1, E')$ from Berkeley I, separating the "good" events from those with anomalously high pulse height in the ΔE_1-detector, 175-2. In this one case, both determinations of Z involve ΔE_1, so the good and bad events are not aligned with each other on either axis. The vertical line extending downward from the "good" Z = 18 events are caused by "edge effects" in the ΔE_2-detector, hence the value of $Z(\Delta E_1, E')$ is correct but $Z(\Delta E_2, \Delta E_1, E')$ is not.

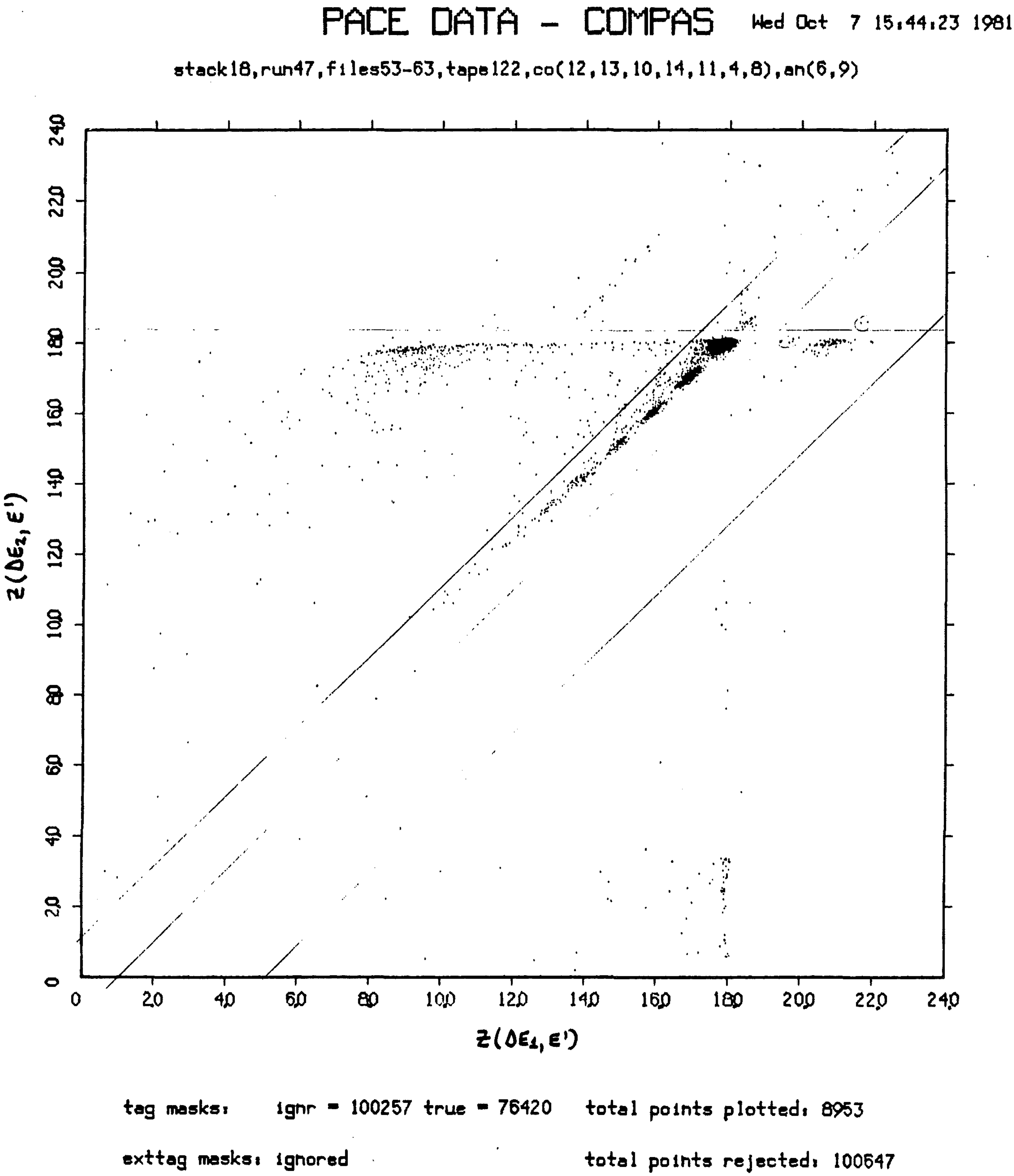

Fig. 13. Cross-plot of $Z(\Delta E_2,E')$ vs. $Z(\Delta E_1,E')$ from Berkeley I, separating the "good" events from those with anomalously high pulse height in the ΔE_1-detector, 175-3.

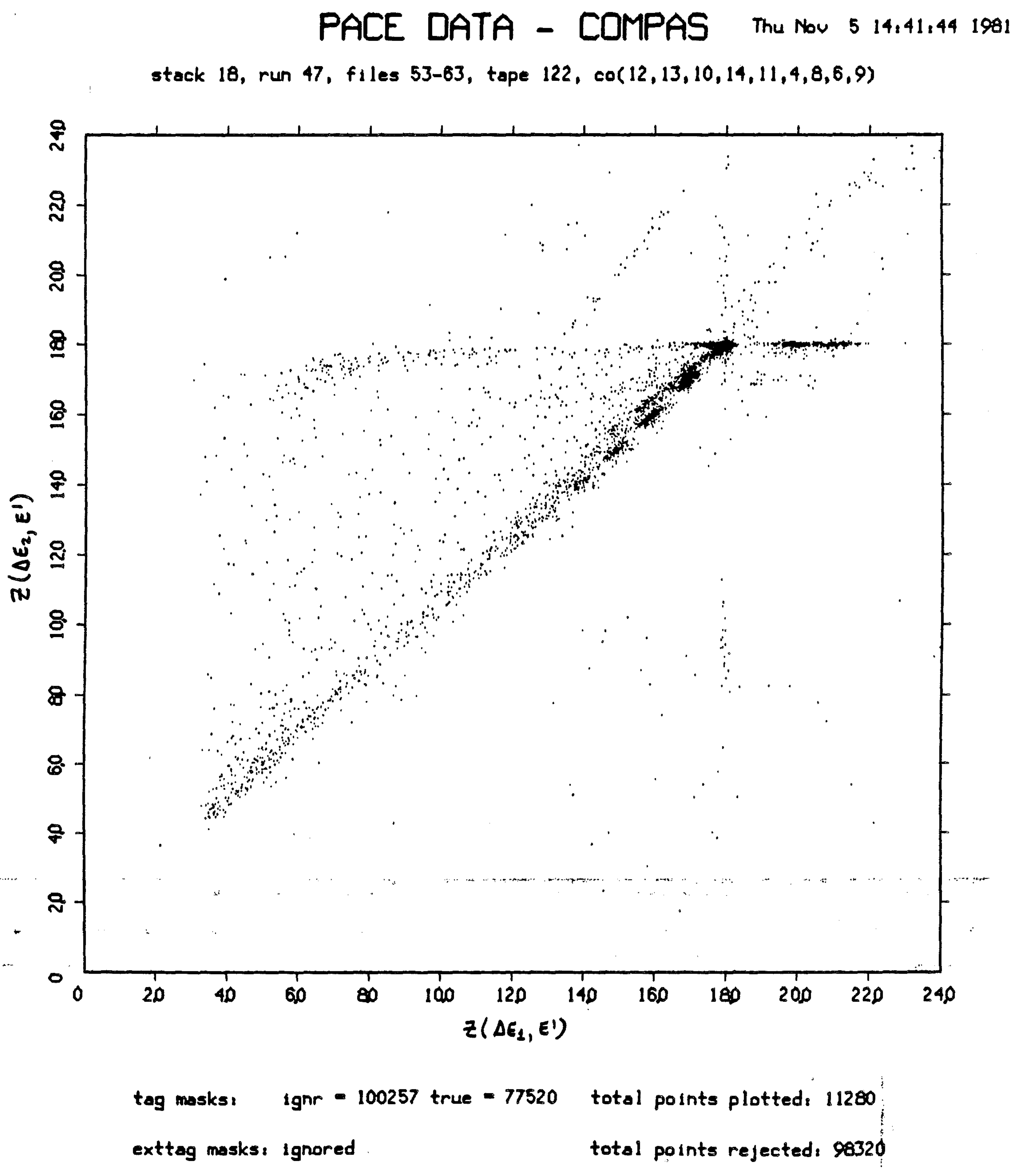

Fig. 14. Cross-plot of $Z(\Delta E_2, E')$ vs. $Z(\Delta E_1, E')$ from Berkeley I, separating the "good" events from those with anomalously high pulse height in the ΔE_1-detector, 175-4.

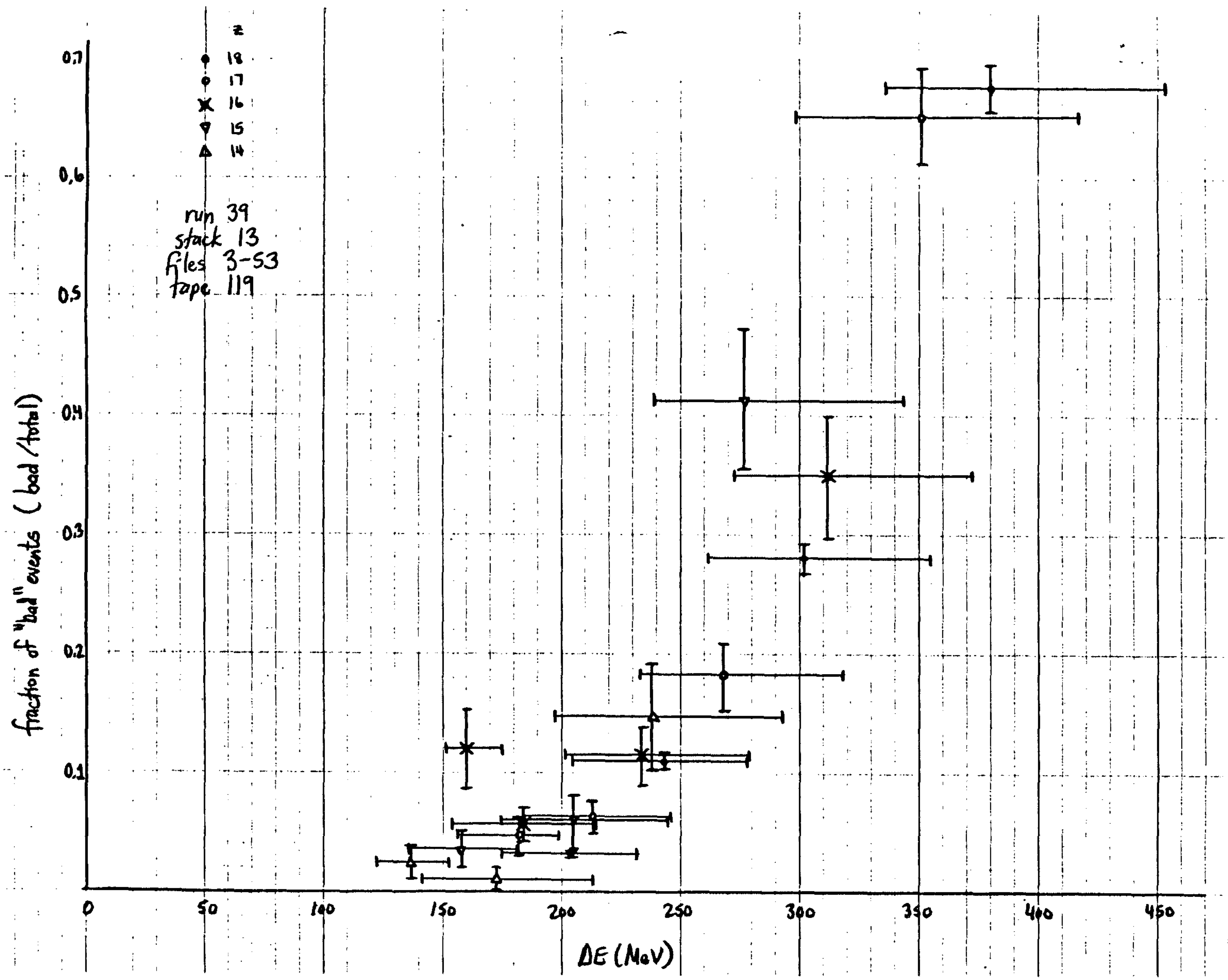

Fig. 15. Bad event fraction (bad events/total events) vs. ΔE_1 for detector 175-2, using Z = 14 through 18 data from Berkeley I. It can be seen that the data for the different elements agree reasonably well.

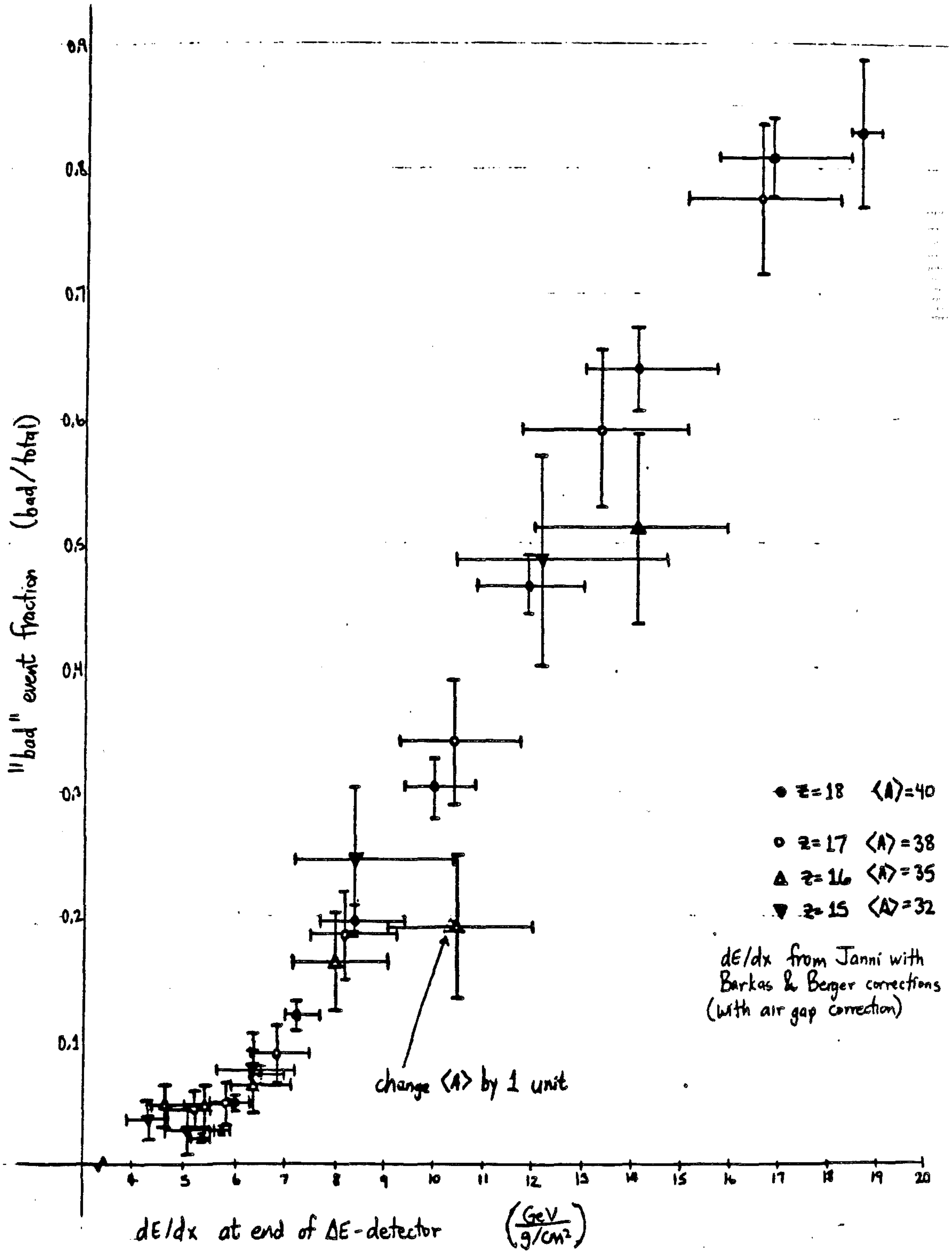

Fig. 16. Bad event fraction (bad events/total events) vs. dE/dx at the back (aluminum) side of ΔE_1-detector 175-2, using Z = 15 through 18 data from Berkeley I. Note the good agreement between the data for different elements.

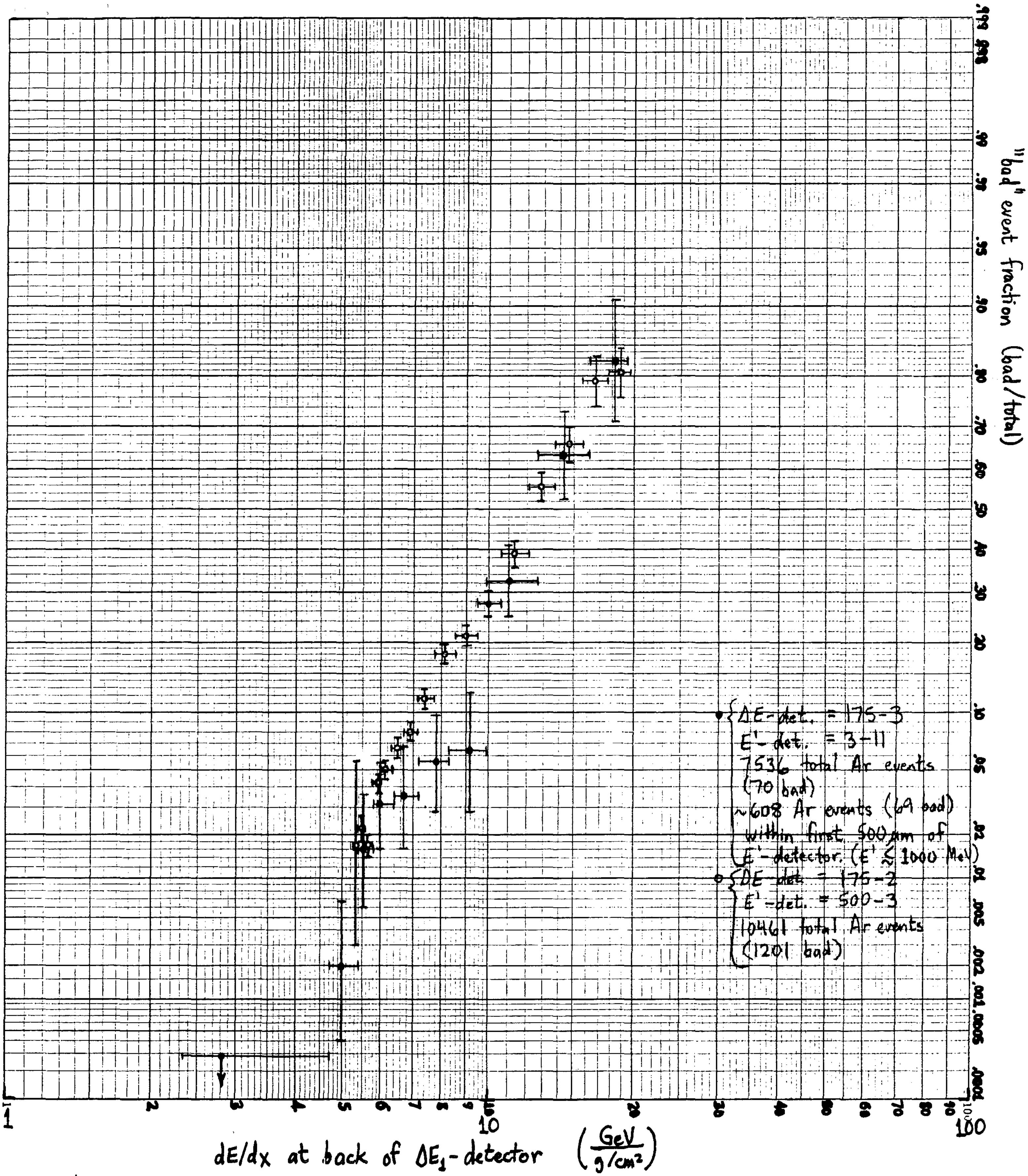

Fig. 17. Bad event fraction (bad events/total events) vs. dE/dx at the back (aluminum) side of the ΔE_1 detector in Berkeley I (Z = 18 only), for ΔE_1 detectors 175-2 and 175-3.

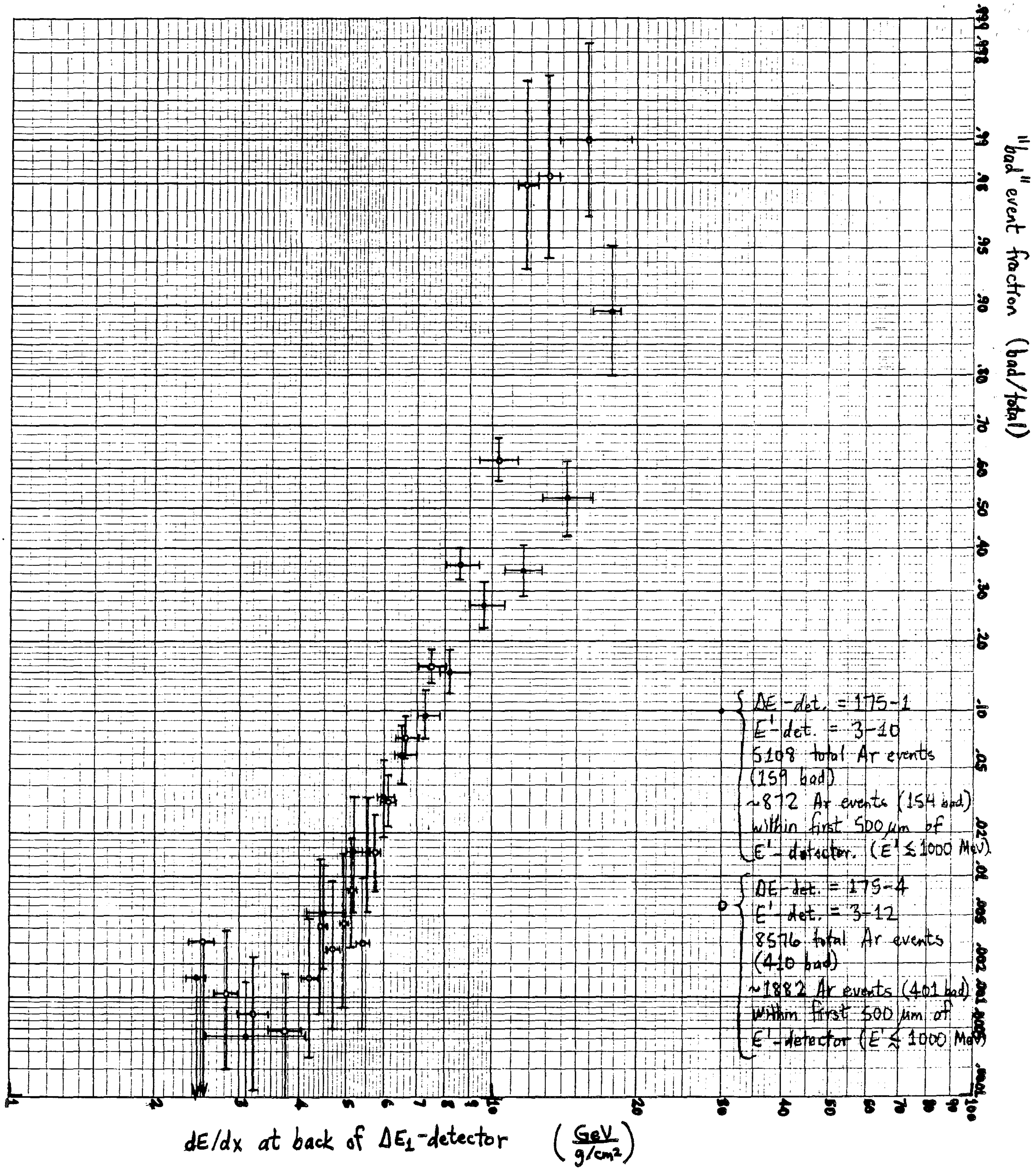

Fig. 18. Bad event fraction (bad events/total events) vs. dE/dx at the back (aluminum) side of the ΔE_1 detector in Berkeley I (Z = 18 only), for ΔE_1 detectors 175-1 and 175-4. Note the apparent difference in shape of the curves for the two detectors.

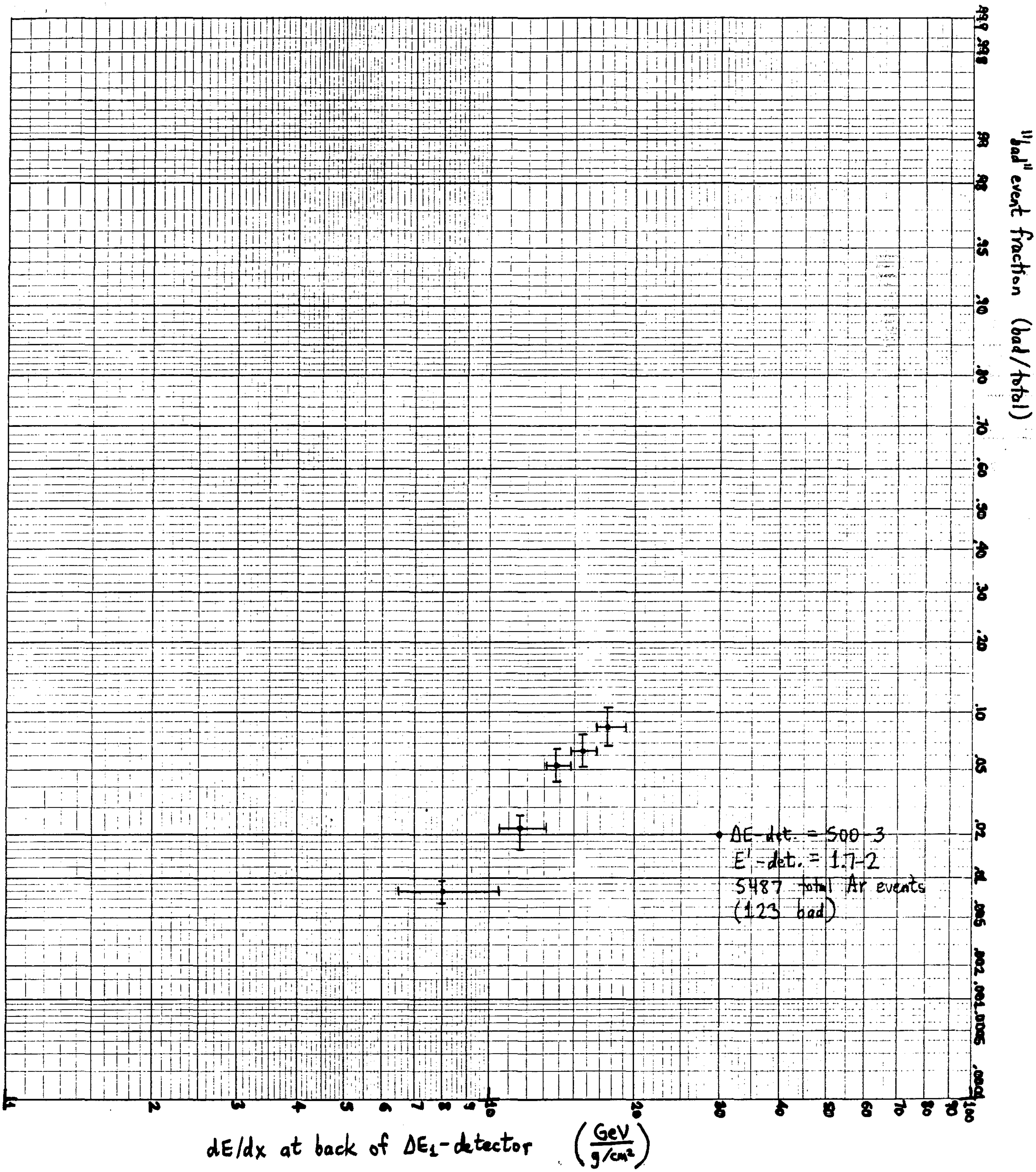

Fig. 19. Bad event fraction (bad events/total events) vs. dE/dx at the back (aluminum) side of the ΔE_1 detector in Berkeley I (Z = 18 only), for ΔE_1 detector 500-3.

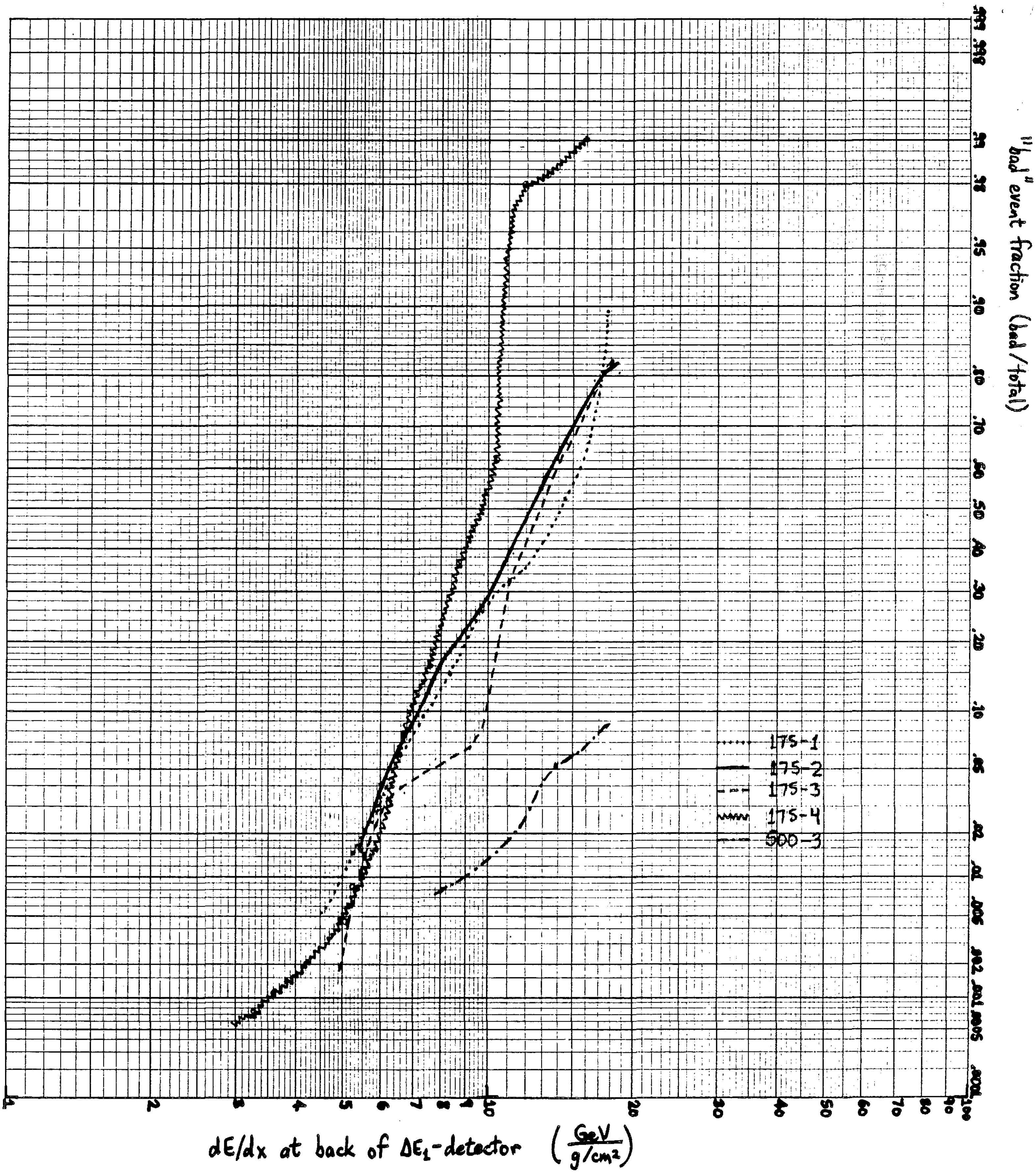

Fig. 20. Comparison of bad event fraction vs. dE/dx for the five detectors studied in Berkeley I. Note that three of the 175-μm detectors appear comparable, while the fourth is much worse, and that the 500-μm detector shows fewer bad events than any of the 175-μm detectors.

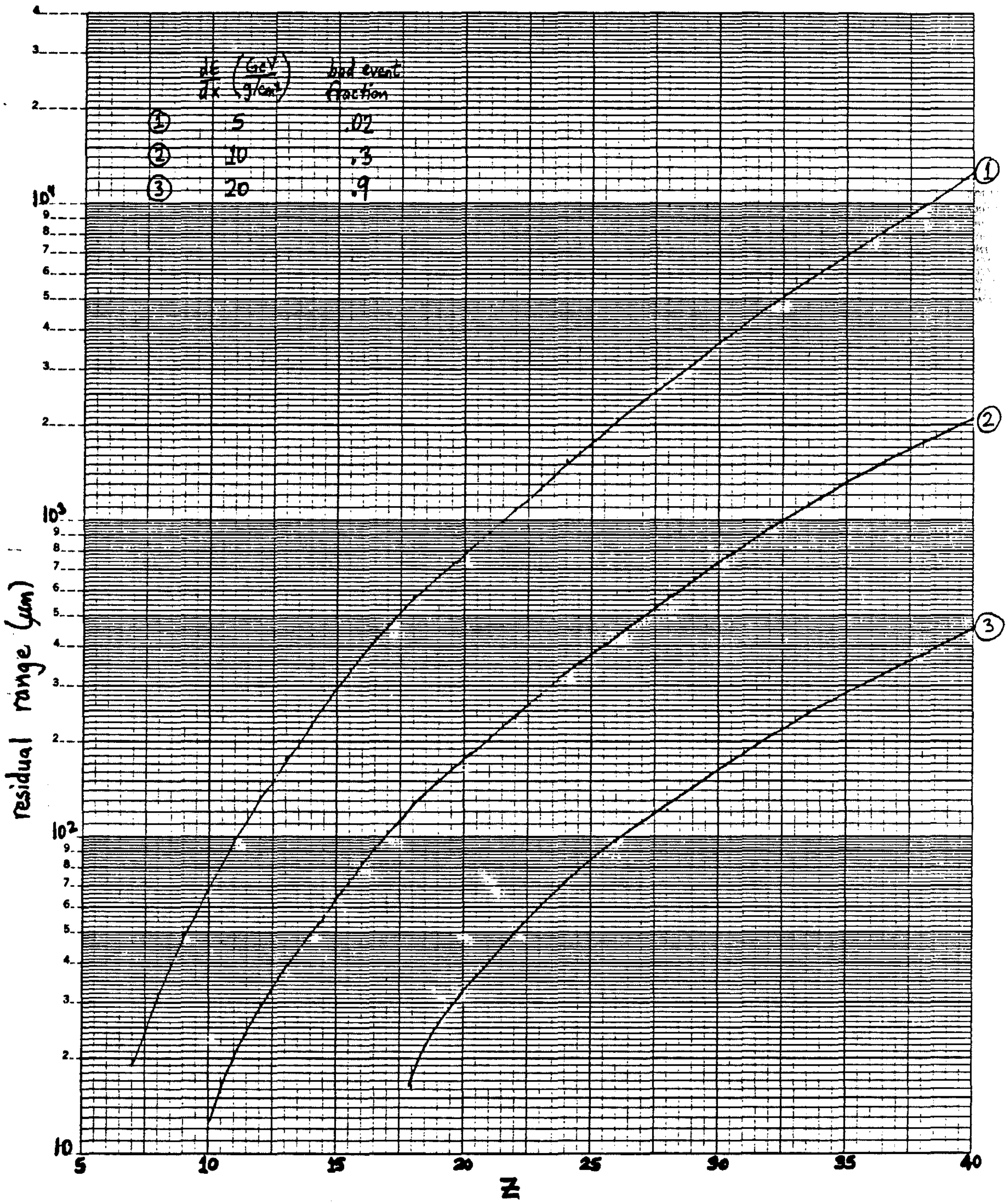

Fig. 21. Residual range (depth in the E'-detector) vs. Z at three values of dE/dx for COMPAS 175-μm detector 175-2, a typical case. Value of bad event fraction corresponding to each dE/dx was obtained from the curve for detector 175-2 in Fig. 20. An average value of A has been assumed for each Z.

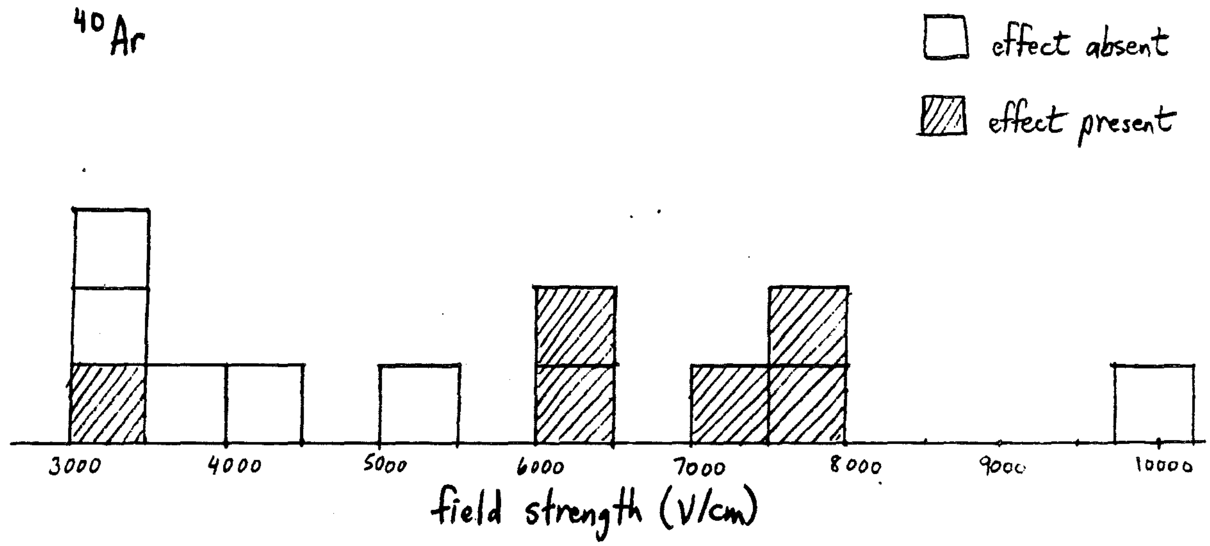

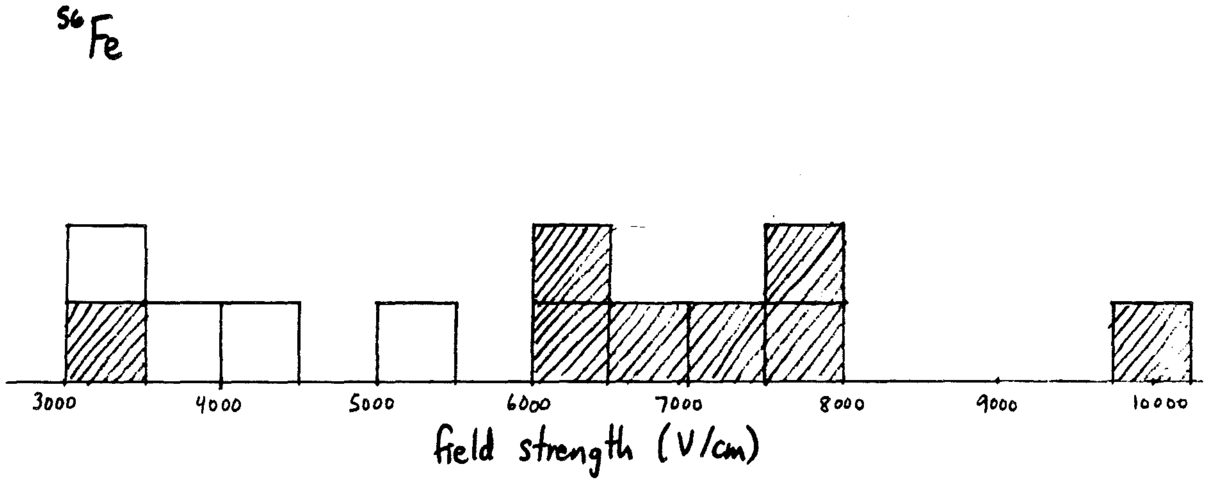

detectors	field strength (V/cm)	side facing beam
2 HIST 50-μm	4250, 5320	Au
1 HIST 90-μm	~3400	Au, Al
2 HIST 150-μm	6000, 6600	Au, Al
1 HIST 500-μm	~3900	Au, Al
16 Voyager LET 35-μm	~10,000	?
4 MAST 115-μm	~3200	Au
4 MAST 175-μm	6010, 7130, 7750, 7800	Au, Al
1 MAST 500-μm	3310	Au

Fig. 22. Histograms of average electric field strength for all SRL surface barrier detectors which have been examined for the multiplication effect with ^{40}Ar or ^{56}Fe particles. The effect was assumed to be present for ^{56}Fe in a given detector even if it was only observed with ^{40}Ar. Other variables, such as detector orientation and p- vs. n-type silicon, have not been taken into account. Note that the effect tends to occur most frequently in detectors with the higher field strengths.

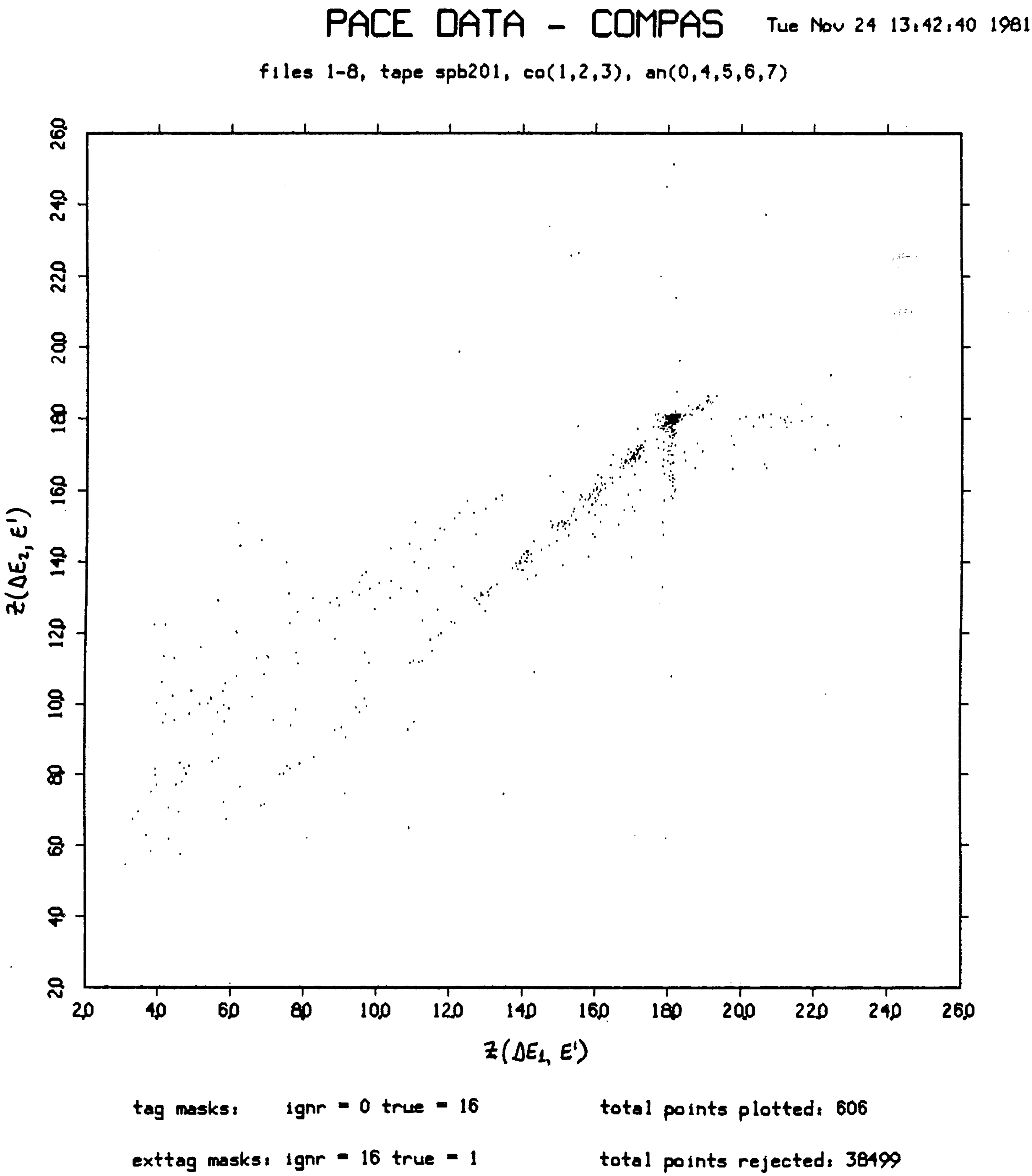

Fig. 23. Cross-plot of $Z(\Delta E_2, E')$ vs. $Z(\Delta E_1, E')$ from Berkeley II, separating the "good" events from those with anomalously high pulse height in the ΔE_1-detector, 175-1. Data for all six biases are included.

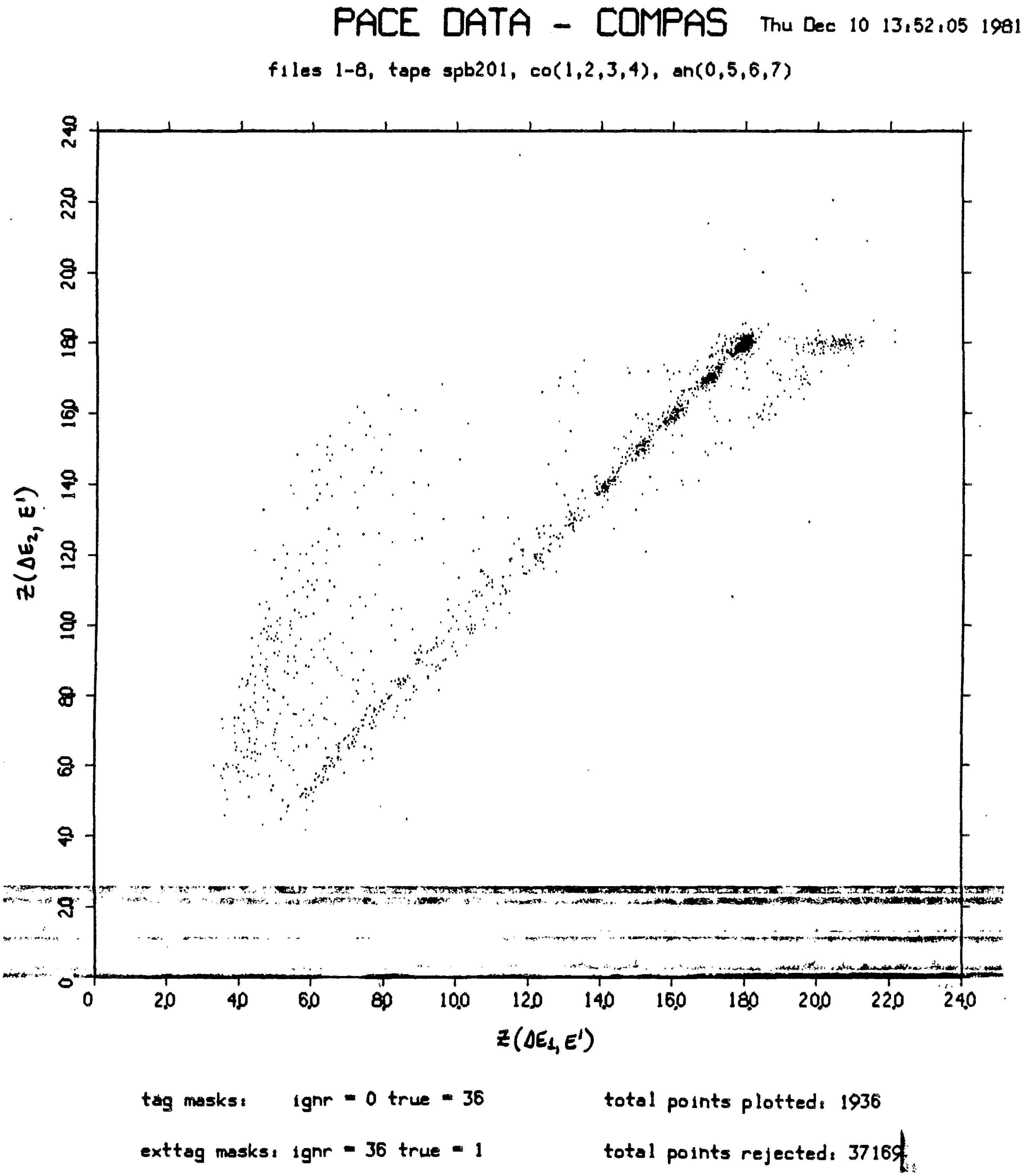

Fig. 24. Cross-plot of $Z(\Delta E_2,E')$ vs. $Z(\Delta E_1,E')$ from Berkeley II, separating the "good" events from those with anomalously high pulse height in the ΔE_1-detector, 175-2. Data for all six biases are included.

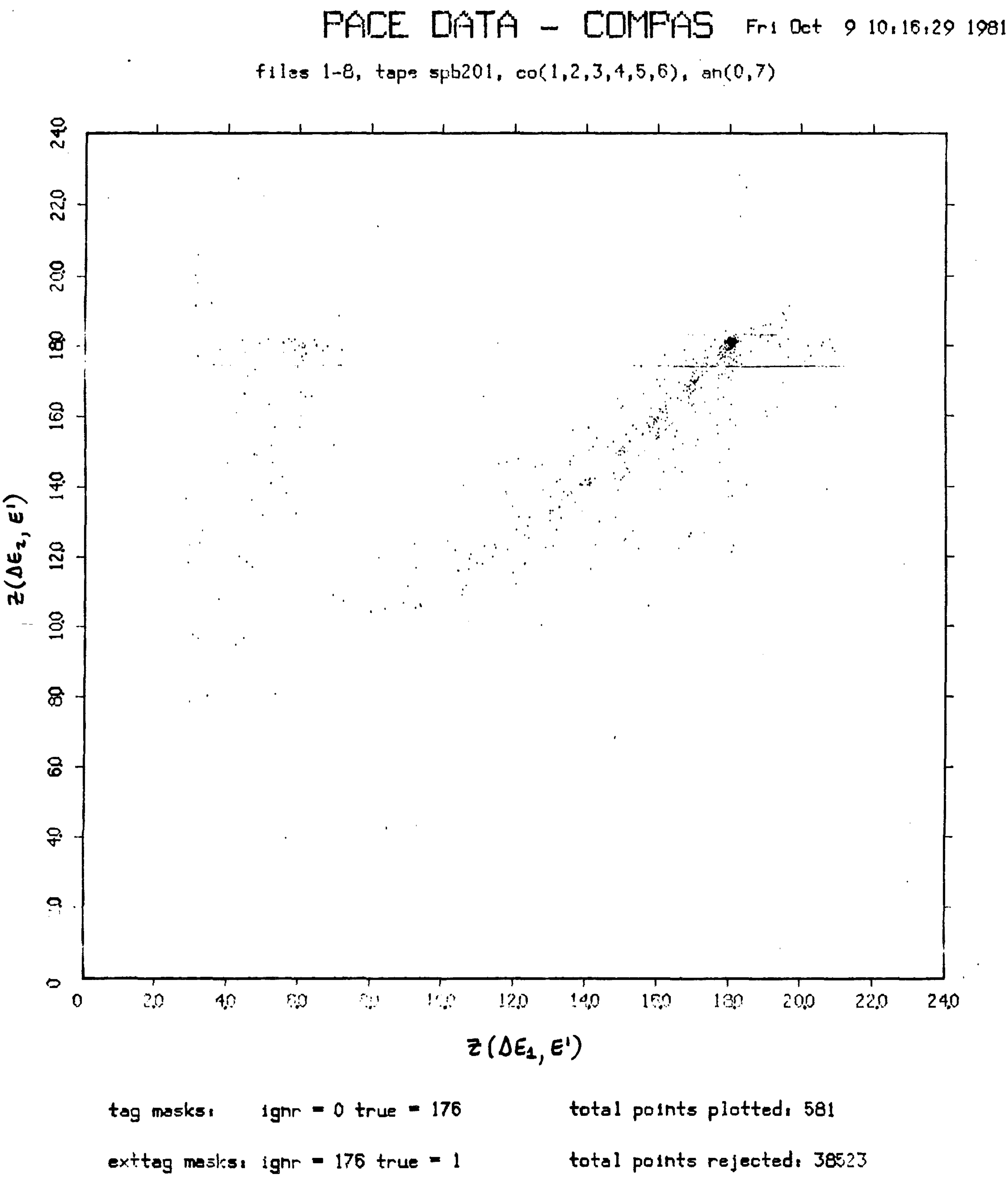

Fig. 25. Cross-plot of $Z(\Delta E_2, E')$ vs. $Z(\Delta E_1, E')$ from Berkeley II, separating the "good" events from those with anomalously high pulse height in the ΔE_1-detector, 175-3. Data for all six biases are included.

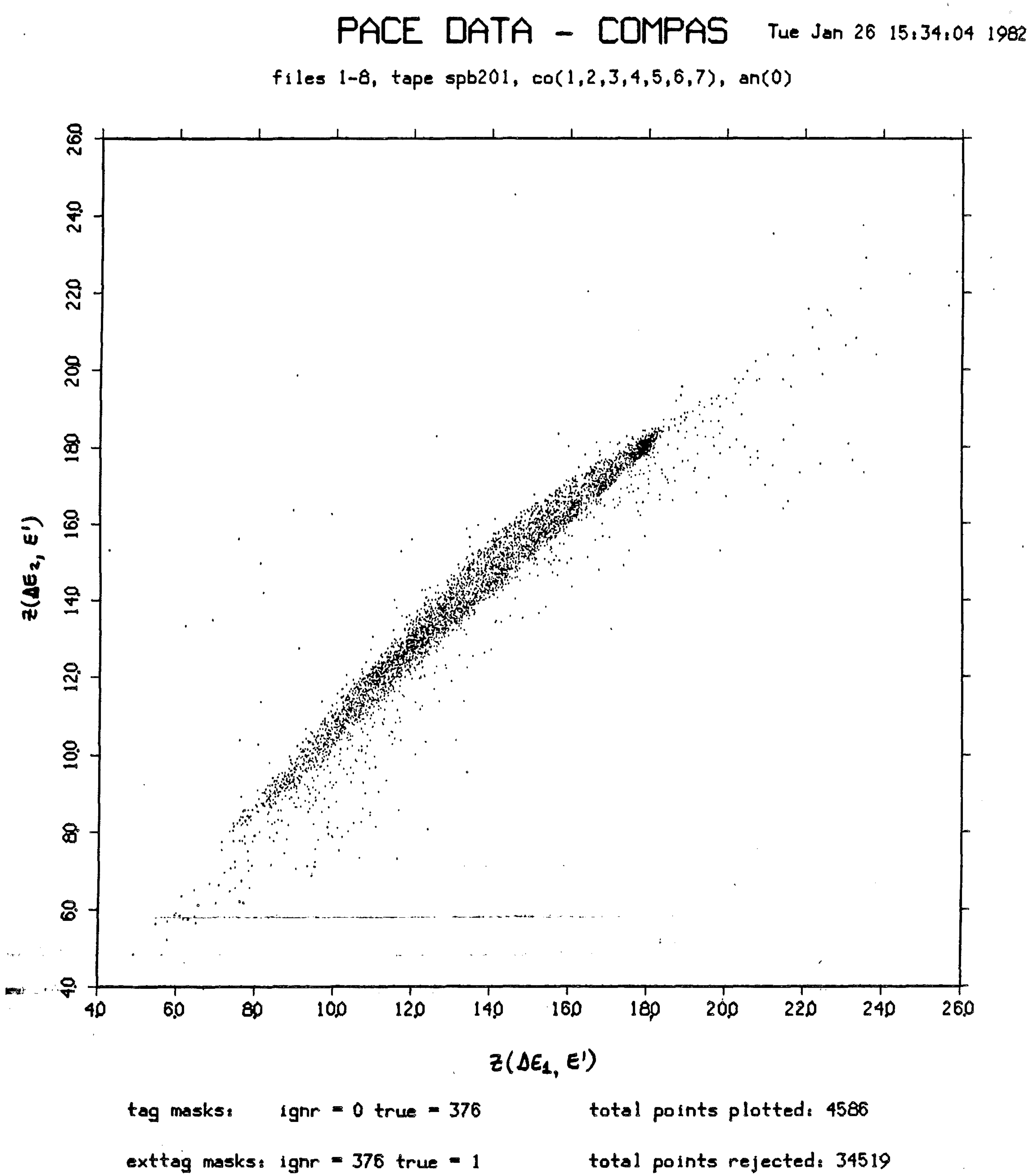

Fig. 26. Cross-plot of $Z(\Delta E_2,E')$ vs. $Z(\Delta E_1,E')$ from Berkeley II, separating the "good" events from those with anomalously high pulse height in the ΔE_1-detector, 175-4. Data for all six biases are included. The severe background problem for this case is believed to be due to an electronic problem. In addition, in Berkeley II there was no way to distinguish events stopping in the last pulse-height-analyzed detector (the E'-detector in this case) from penetrating events.

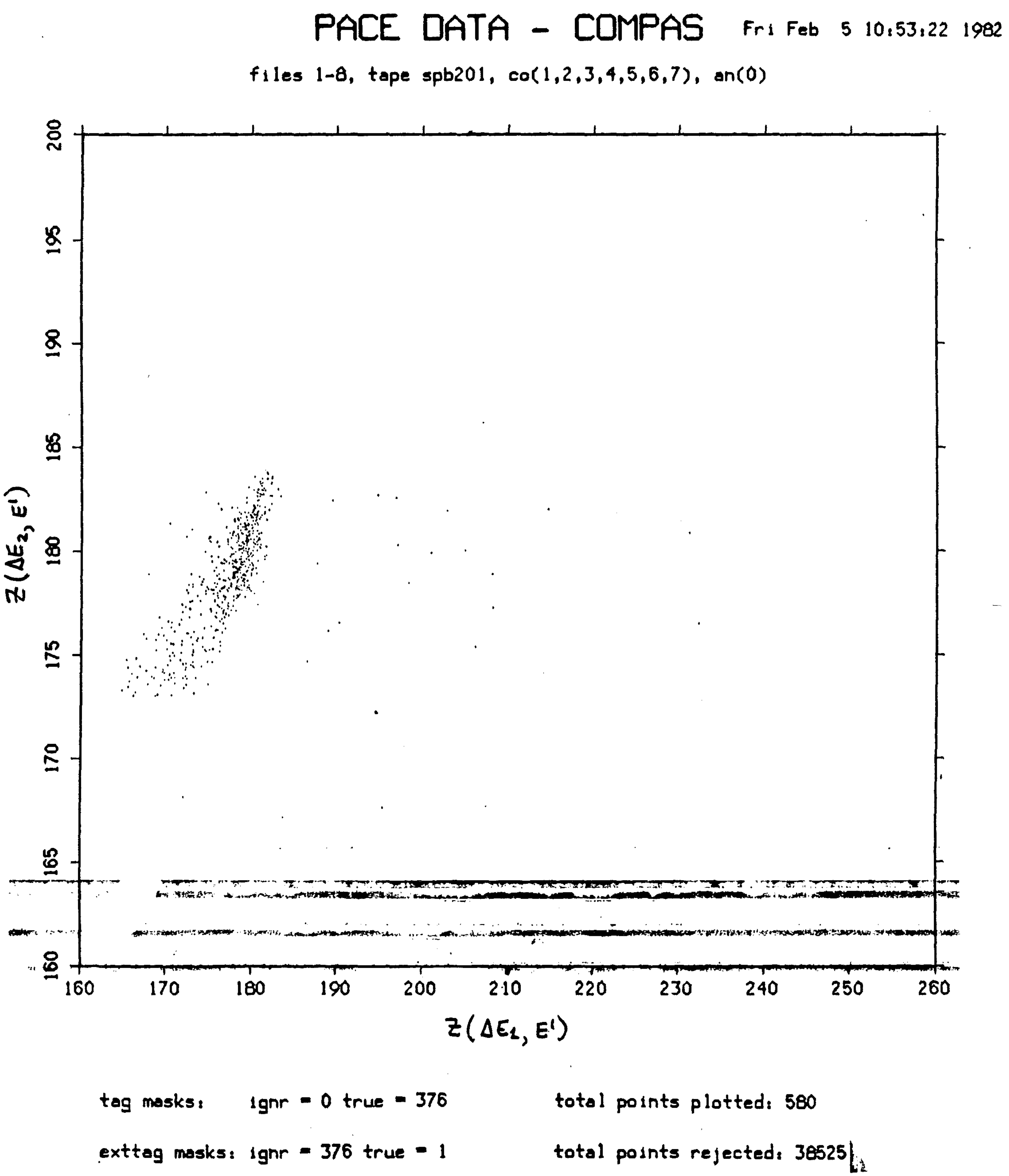

Fig. 27. An enlargement of Fig. 26, showing only the Z = 18 subset of the data included in this analysis.

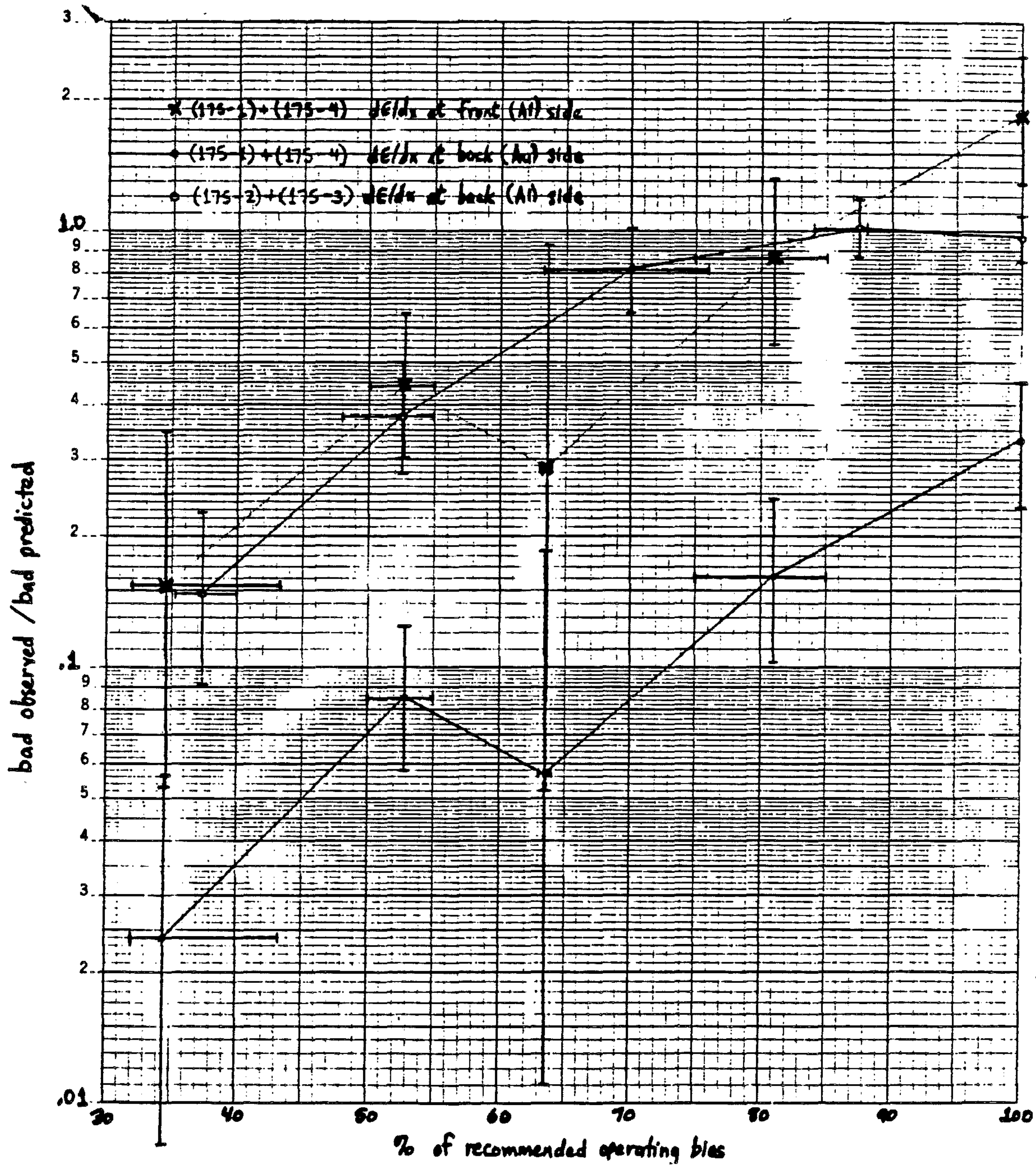

Fig. 28. Ratio of observed to predicted "bad" events vs. bias voltage, summarizing the Berkeley II bias-variation data for the 175-μm detectors. Data with similar biases, and with ΔE_1-detectors in the same orientation with respect to the beam, have been combined to improve event statistics for the points plotted. The effects of lowered bias and of detector orientation are both evident; a bias reduction to about 50% of the recommended bias results in a decrease in the occurrence of the multiplication effect of about a factor of three, and reversal of detectors, so that the aluminum side faces outward, reduces the effect by about a factor of 6 compared to the same detectors in the opposite orientation. Note that the observed/predicted ratios, where the prediction is based on dE/dx at the aluminum surface of the detector, do not agree perfectly for the two sets of detectors in opposite orientations, suggesting that more than just the aluminum surface is involved in generating the multiplication effect.

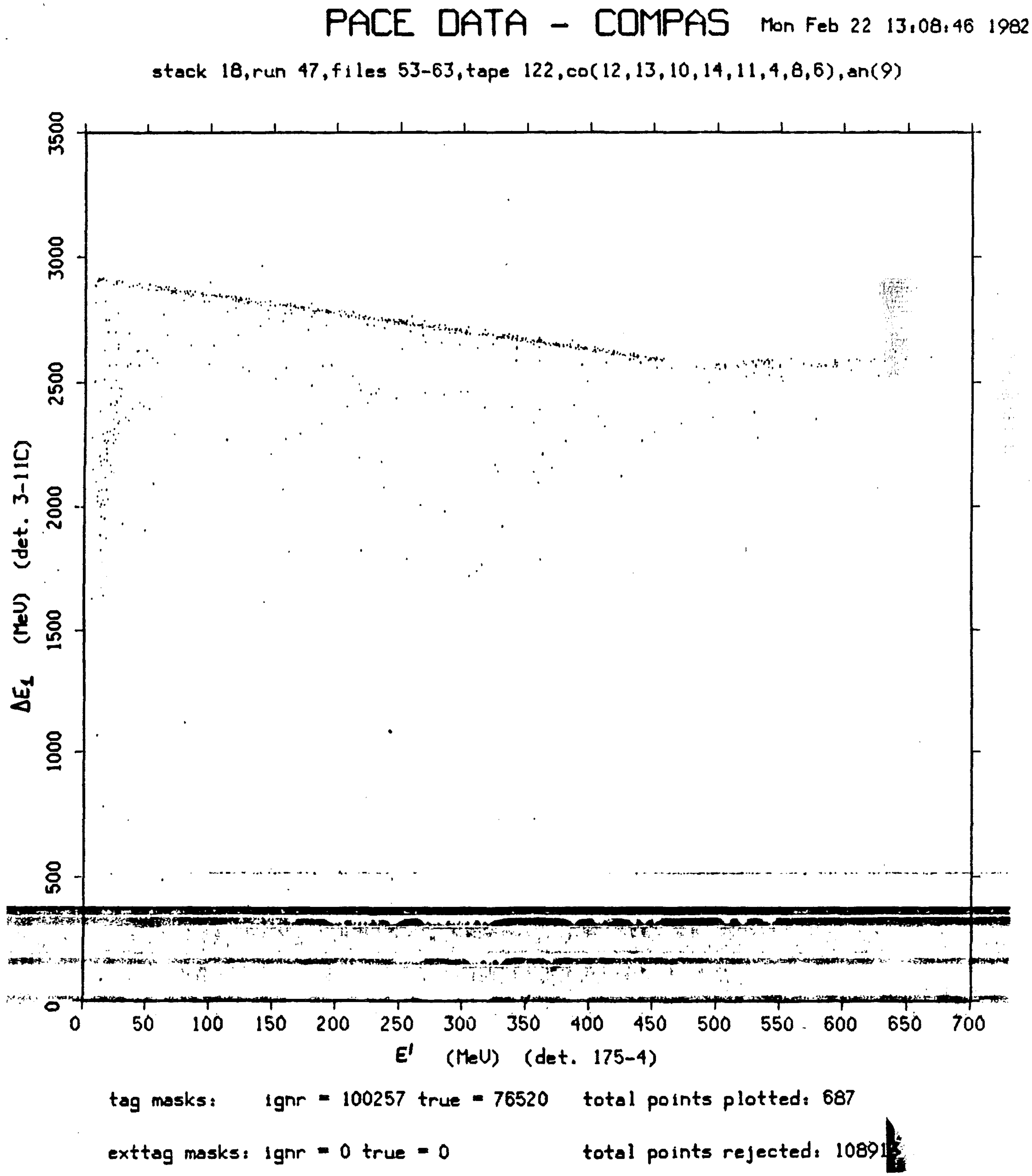

Fig. 29. Scatter-plot of ΔE_1 (detector 3-11) vs. E' (detector 175-4) from Berkeley I. Note the apparent absence of the multiplication effect, showing that it does not occur for events stopping in a 175-μm detector when the gold side faces the beam. In particular, no bad events are seen where the "normal" energy loss in detector 175-4 is ~200-450 MeV, the energy loss range where the multiplication effect was predominant when the same detector was the ΔE_1-detector (compare Fig. 6). The cluster of events at the right edge is the multiplication effect occurring in the "fold-back" part of the element track; they are actually penetrating events. The "double-valued" nature of the effect in this detector, previously noted in Fig. 6, is also evident here.

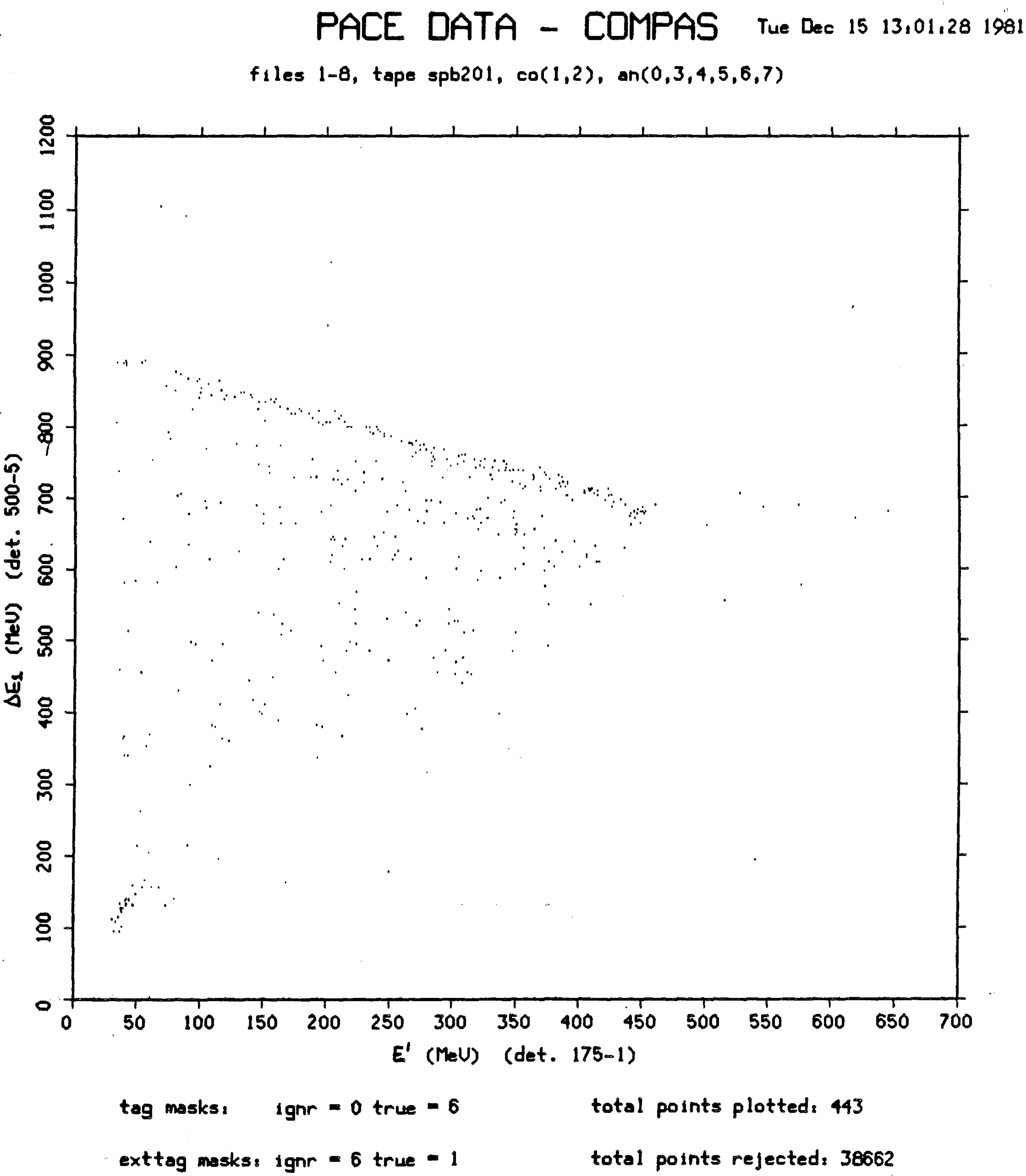

Fig. 30. Scatter-plot of ΔE_1 (detector 500-5) vs. E' (detector 175-1) from Berkeley II. Note the apparent absence of the multiplication effect, showing that it does not occur for events stopping in a reversed 175-μm detector. In particular, no bad events are seen where the "normal" energy loss in detector 175-1 is ~250-400 MeV, the energy loss range where the multiplication effect was predominant when the same detector was the ΔE_1-detector and in the opposite orientation (compare Fig. 3). The cluster of events at the right edge is the multiplication effect occurring in the "fold-back" part of the element track; they are actually penetrating events.

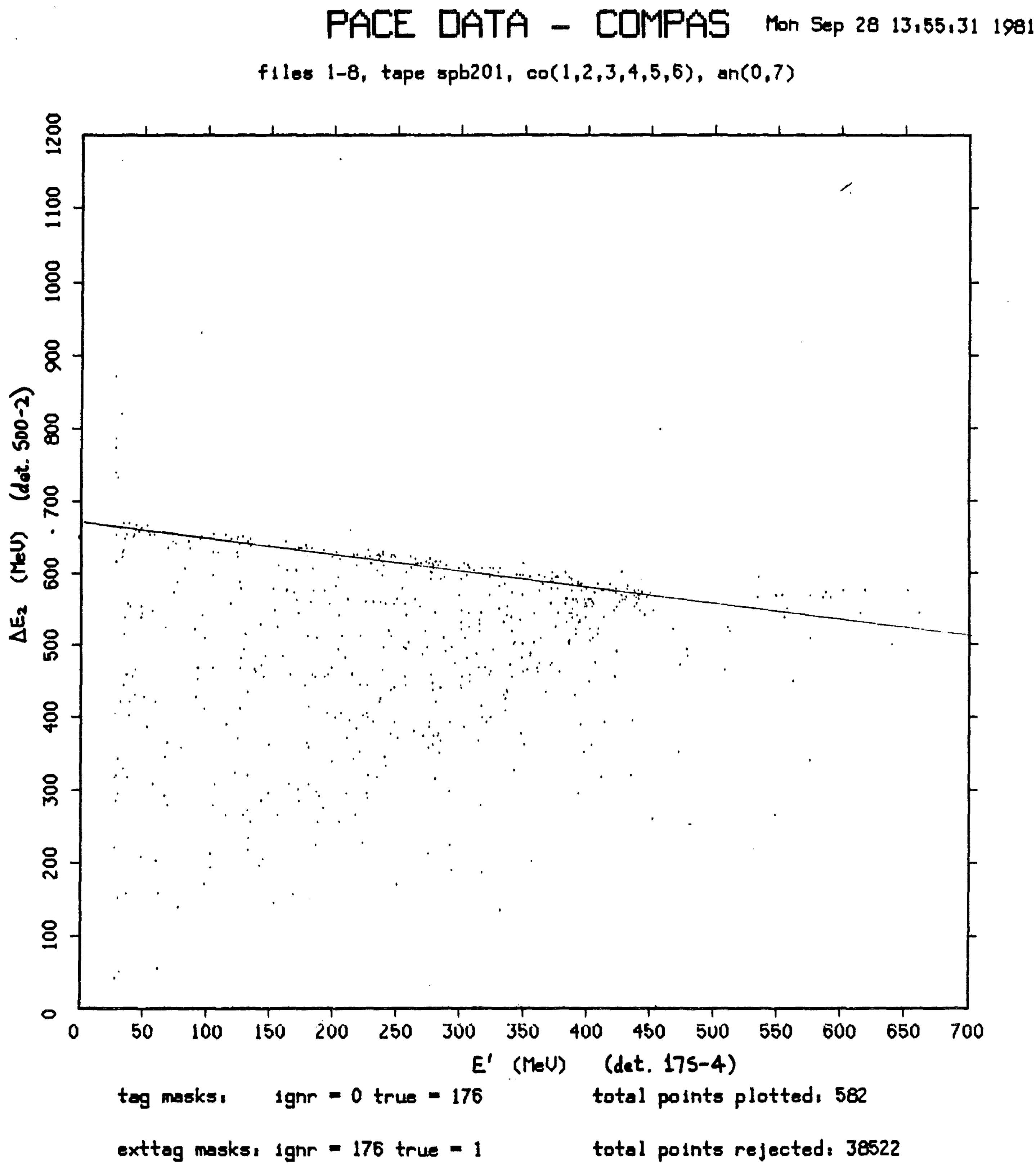

Fig. 31. Scatter-plot of ΔE_2 (detector 500-2) vs. E' (detector 175-4) from Berkeley II. The apparent absence of the multiplication effect shows that it does not occur for events stopping in a reversed 175-μm detector. In particular, no bad events are seen where the "normal" energy loss in detector 175-4 is ~200-450 MeV, the energy loss range where the multiplication effect was predominant when the same detector was the ΔE_1-detector and in the opposite orientation (compare Fig. 6). The cluster of events at the right edge is the effect occurring in the "fold-back" part of the element track; they are actually penetrating events. The ΔE_1-detector (175-3) was not used here because this detector shows the effect to a degree comparable to the E'-detector being studied.

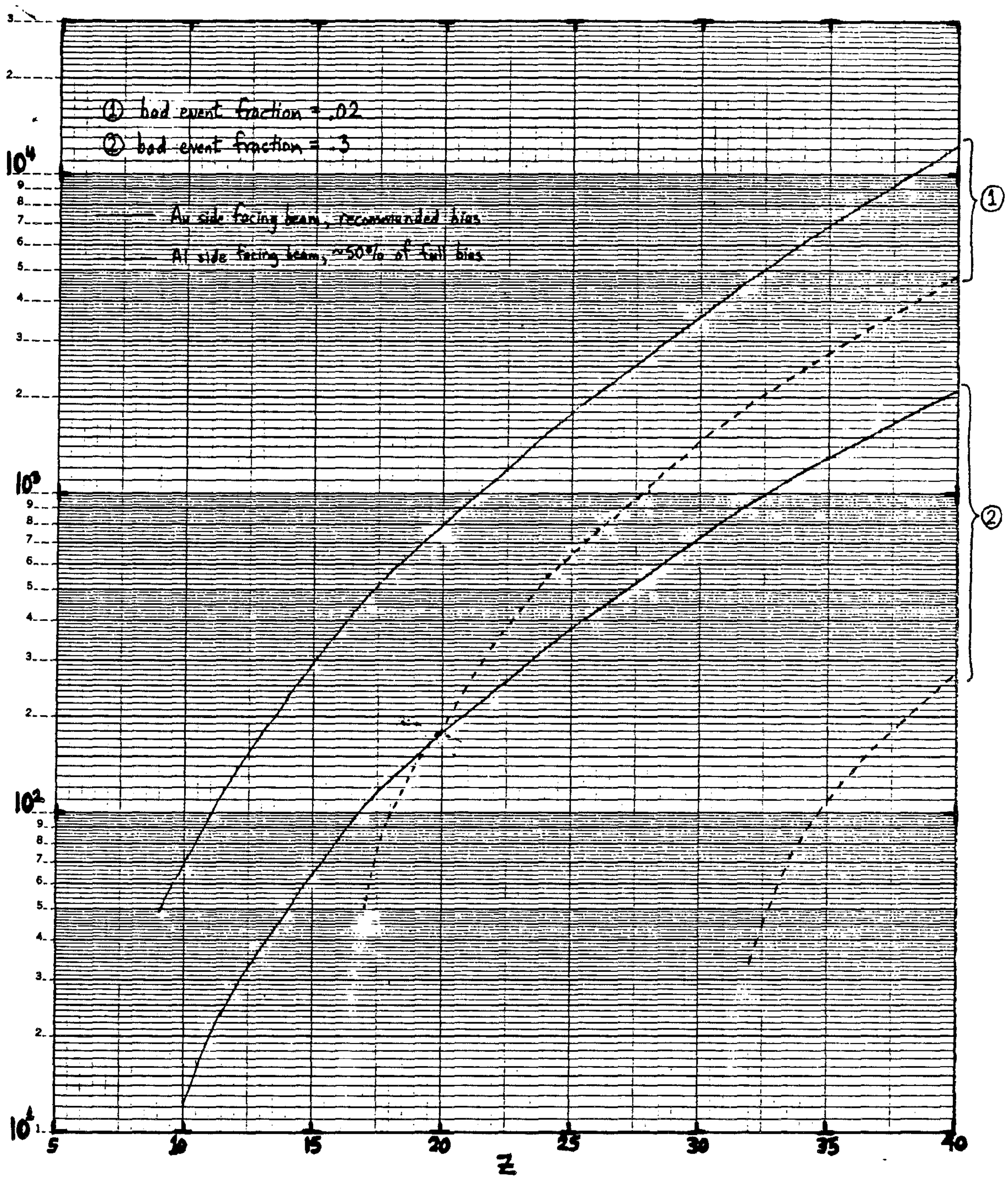

Fig. 32. Residual range vs. Z for bad event fraction at the 2% and 30% levels for the COMPAS 175-μm detector 175-2. The solid curves are reproduced from Fig. 21; the dashed curves are the corresponding curves when both 50% bias reduction and detector orientation reversal are implemented. The considerable improvement provided by these two measures is evident. A factor of three reduction in bad events due to the lower bias was obtained from Fig. 28 and is an average over the energy range involved in this study; here it was assumed that this factor holds for all energies. A further reduction in residual range of 175 μm due to detector reversal was then applied, reflecting the assumption that dE/dx at the aluminum surface of the detector is the only important quantity affecting the magnitude of the multiplication effect in a given detector.

Appendix A. Examples of scatter-plots exhibiting various aspects of the pulse height multiplication effect, taken from the HIST detector Berkeley Bevalac calibration data (Ref. 2). This data provides evidence for the effect occurring in the two 150-μm detectors. The plots included here show the effect occurring in detector 150-1 as the ΔE_1-detector (in both orientations), its absence in the same detector as the E'-detector (again in both orientations), its angular dependence for this detector in the "reversed" orientation, and its occurrence in "reversed" detector 150-2.

HIST Bevalac #2
1976 ^{40}Ar Calibration

Au 90-2
Au 150-1
Au 500-6

7511 EVENTS

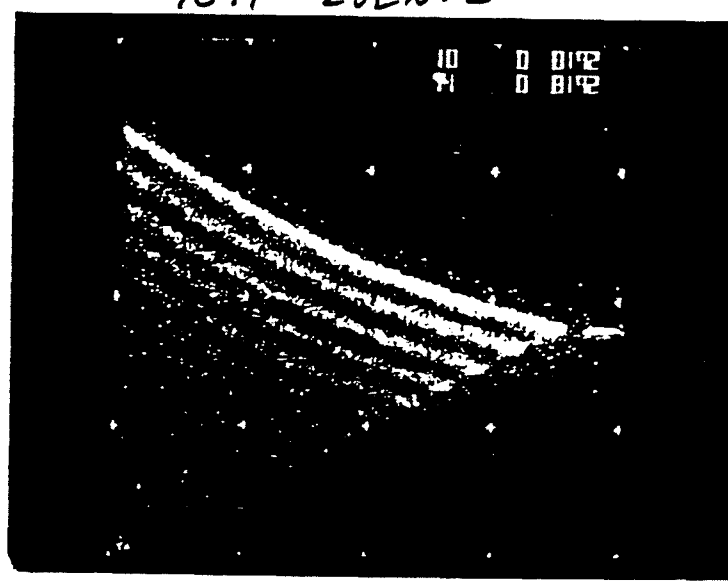

HBKZZO

90-2 vs 150-1

32,341 EVENTS

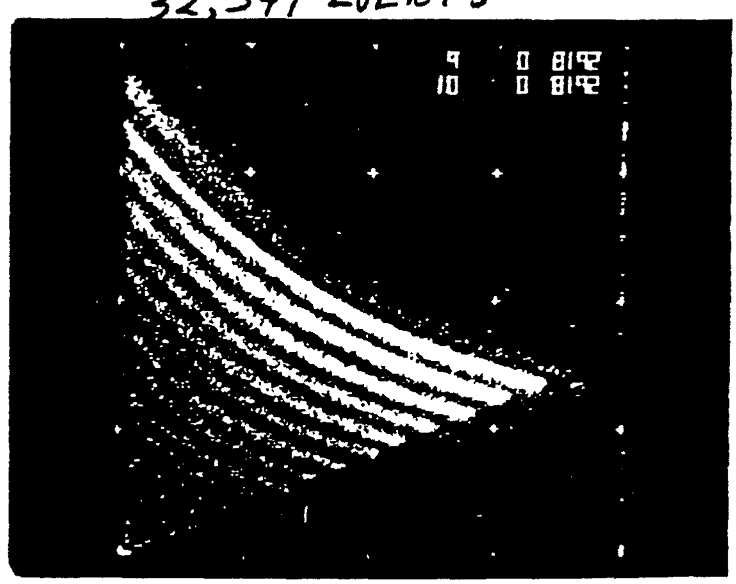

HBKZZO

150-1 vs 500-6

HIST Fe Calibration - Flight Instrument July 1977

D1 —— Al —— 90-2

D2 —— Al —— 150-1

D3 —— Al —— 500-6

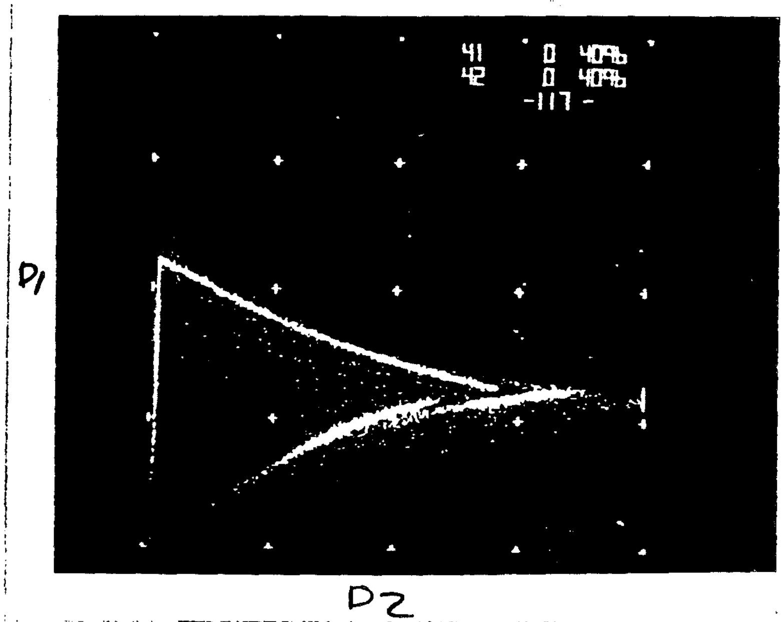

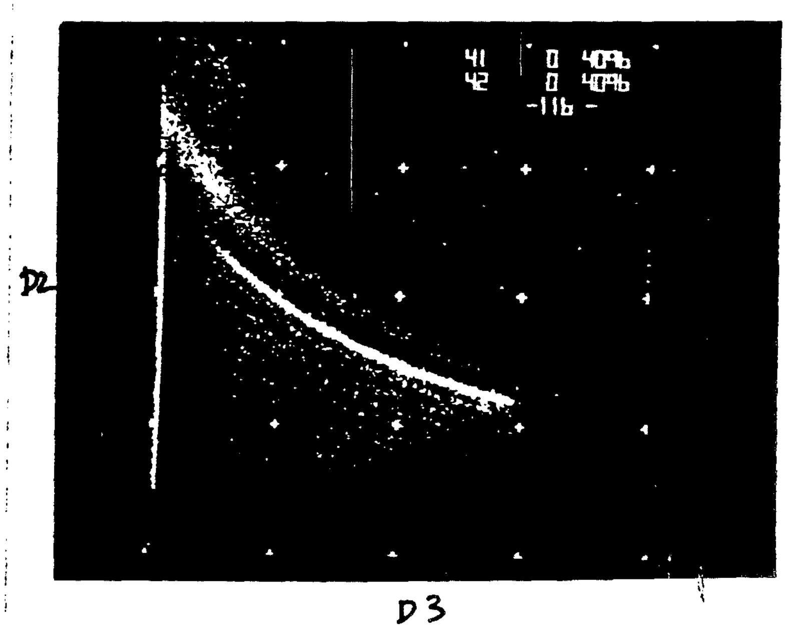

H15T Fe Calibration 7/77

D2

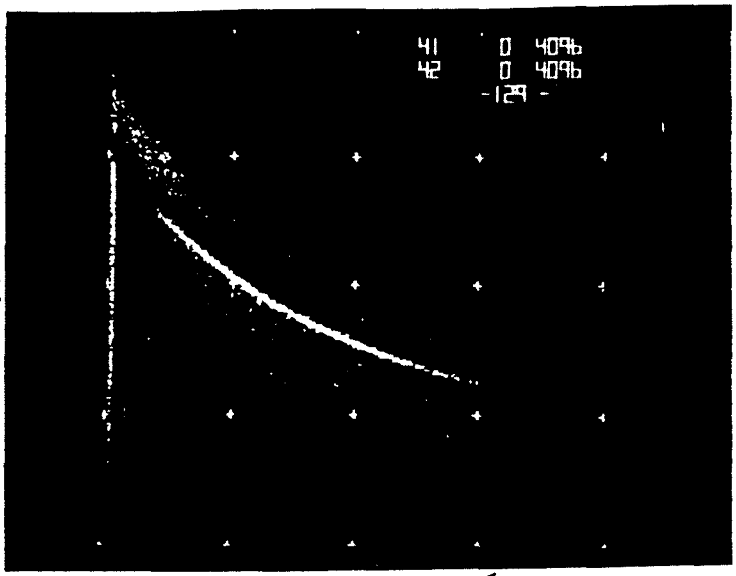

D3 -20°

D2

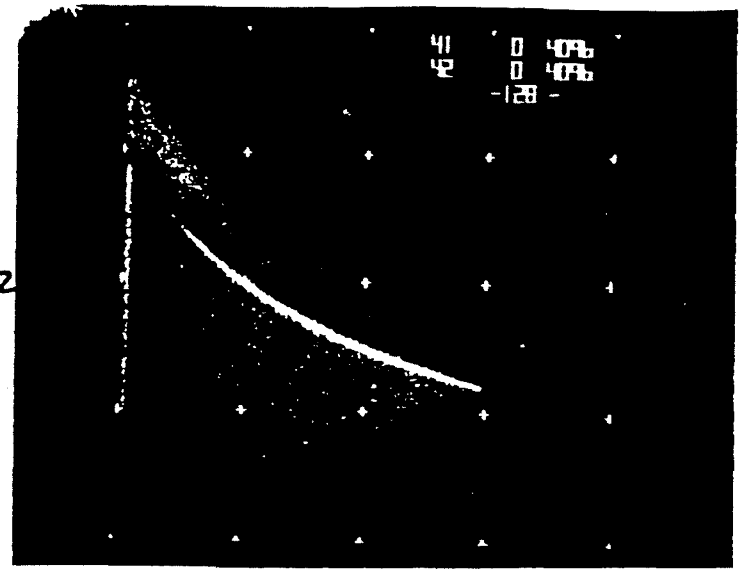

D3 -10°

D2

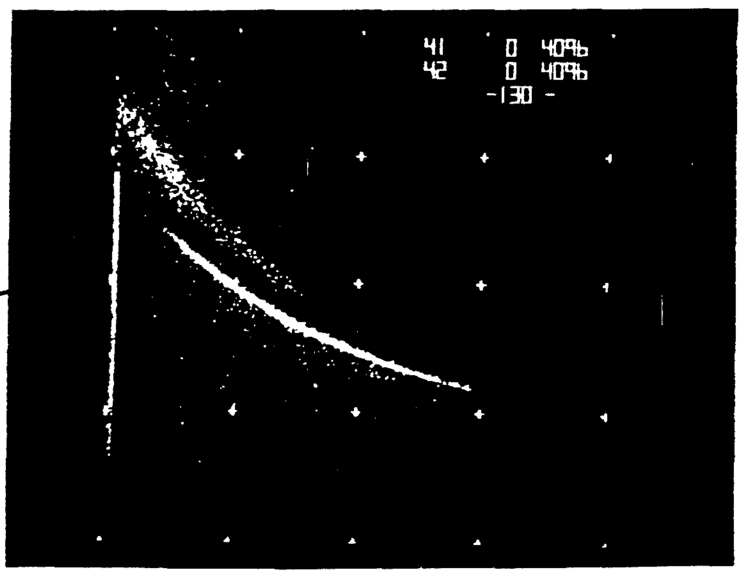

D3 0°

D2

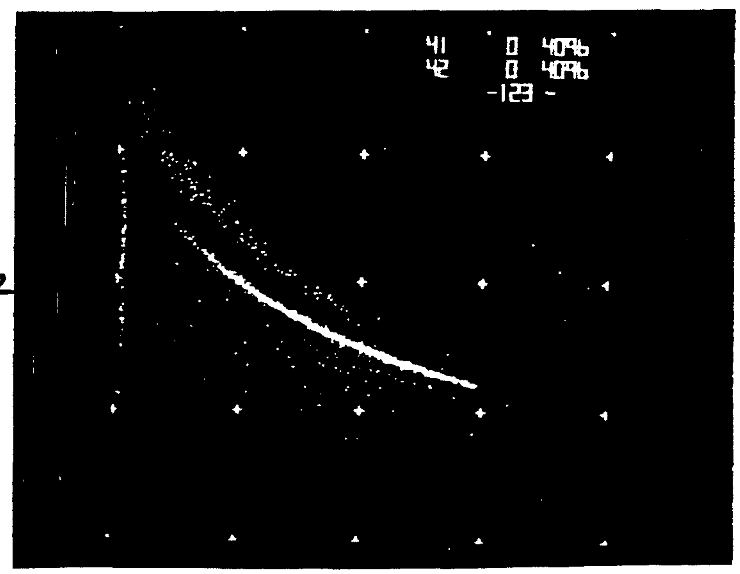

D3 +10°

D2

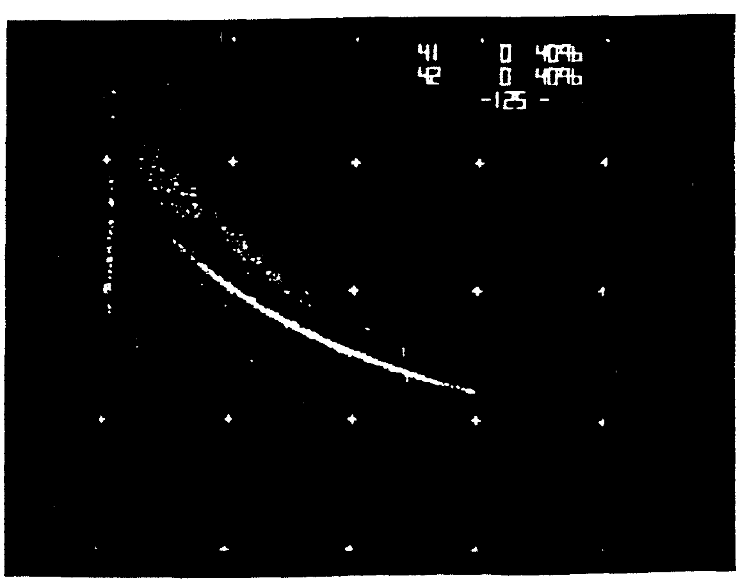

D3 +15°

D2

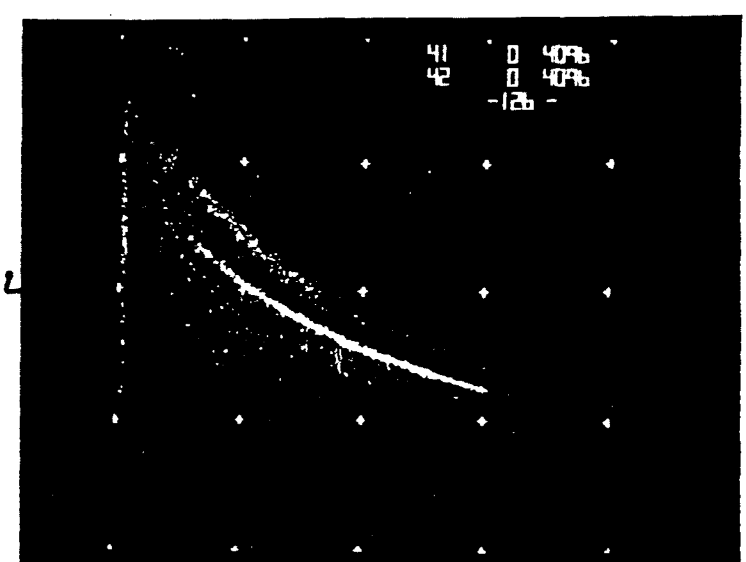

D3 +20°

HIST Fe Calib,

Flight. Inst.

April 1978

D1 —— Al —— 90-2

D2 —— Al —— 150-2

D3 —— Al —— 500-6